This is the postprint (accepted) version of the final paper, published afterwards, here: https://doi.org/10.1016/j.ejmech.2020.112047

We thank Elsevier for the opportunity.

Identification of a 2,4-diaminopyrimidine scaffold targeting *Trypanosoma brucei* pteridine reductase 1 from the LIBRA compound library screening campaign.

Pasquale Linciano,[1] Gregorio Cullia,[2] Chiara Borsari,[1†] Matteo Santucci,[1] Stefania Ferrari,[1] Gesa Witt,[3] Sheraz Gul,[3] Maria Kuzikov,[3] Bernhard Ellinger,[3] Nuno Santarém,[4] Anabela Cordeiro da Silva,[4,12] Paola Conti,[2] Maria Laura Bolognesi,[5] Marinella Roberti,[5] Federica Prati,[5] Francesca Bartoccini,[7] Michele Retini,[6] Giovanni Piersanti,[6] Andrea Cavalli,[5,7] Luca Goldoni,[8] Sine Mandrup Bertozzi,[8] Fabio Bertozzi,[9] Enzo Brambilla,[9] Vincenzo Rizzo,[9] Daniele Piomelli,[10] Andrea Pinto,[11,*] Tiziano Bandiera[9,*] and Maria Paola Costi[1,*]

[1]*Dipartimento di Scienze della Vita, University of Modena and Reggio Emilia, Via Campi 103, 41125, Modena, Italy.*
[2]*Department of Pharmaceutical Sciences, University of Milan, Via Mangiagalli 25, 20133, Milan, Italy.*
[3]*Fraunhofer Institute for Molecular Biology and Applied Ecology – ScreeningPort, Hamburg, Germany.*
[4]*Institute for Molecular and Cell Biology, 4150-180 Porto, Portugal and Instituto de Investigação e Inovação em Saúde, Universidade do Porto, 4150-180, Porto, Portugal.*
[5]*Department of Pharmacy and Biotechnology, Alma Mater Studiorum-University of Bologna, Via Belmeloro 6, I-40126 Bologna, Italy.*
[6]*Department of Biomolecular Sciences, Section of Chemistry, University of Urbino "Carlo Bo", Piazza Rinascimento 6, 61029 Urbino, Italy.*
[7]*Computational and Chemical Biology, Istituto Italiano di Tecnologia, Via Morego 30, I-16163 Genova, Italy.*
[8]*Analytical Chemistry Facility, Istituto Italiano di Tecnologia, Via Morego 30, I-16163 Genova, Italy*
[9]*PharmaChemistry Line, Istituto Italiano di Tecnologia, Via Morego 30, I-16163 Genova, Italy.*
[10]*Departments of Anatomy and Neurobiology, Pharmacology and Biological Chemistry, University of California, Irvine 92697-4625, USA.*
[11]*Department of Food, Environmental and Nutritional Sciences, University of Milan, Via Celoria 2, 20133 Milan, Italy.*
[12]*Department of Biological Sciences, Faculty of Pharmacy, University of Porto.*

KEYWORDS

LIBRA compound library, high throughput screening, anti-parasitic drug discovery, pteridine reductase 1.

ABSTRACT

The LIBRA compound library is a collection of 522 non-commercial molecules contributed by various Italian academic laboratories. These compounds have been designed and synthesized during different medicinal chemistry programs and are hosted by the Italian Institute of Technology. We report the screening of the LIBRA compound library against *Trypanosoma brucei* and *Leishmania major* pteridine reductase 1, *Tb*PTR1 and *Lm*PTR1. Nine compounds were active against parasitic PTR1 and were selected for cell-based parasite screening, as single agents and in combination with methotrexate (MTX). The most interesting *Tb*PTR1 inhibitor identified was 4-(benzyloxy)pyrimidine-2,6-diamine (**LIB_66**). Subsequently, six new **LIB_66** derivatives were synthesized to explore its Structure-Activity-Relationship (SAR) and absorption, distribution, metabolism, excretion and toxicity (ADMET) properties. The results indicate that PTR1 has a preference to bind inhibitors, which resemble its biopterin/folic acid substrates, such as the 2,4-diaminopyrimidine derivatives.

1. Introduction

Screening in drug discovery allows the rapid testing of compound libraries against biological targets implicated in disease processes to identify hit compounds for further medicinal chemistry optimization in the drug discovery value chain [1]. Several drugs currently in clinical trials originate from hits identified during high throughput screening (HTS) campaigns [2,3]. HTS using target-based assays has been extensively used in the drug discovery process for neglected tropical diseases (NTD) [3]. These diseases mainly affect marginalized and economically disadvantaged communities; in addition, they are the major causes of morbidity and mortality in tropical and subtropical regions [4]. Parasites of the *Trypanosomatidae* family are the agents of human and animal vector-borne diseases, including human African trypanosomiasis (HAT), which is caused by *Trypanosoma brucei*, and Leishmaniasis, which is caused by several *Leishmania* spp. [5]. Currently, NTD control relies extensively on chemotherapy and prophylaxis. The available drugs for these diseases were discovered many decades ago and they suffer from many drawbacks, such as toxicity, poor efficacy, and drug resistance [6–8]. Recently, the combination of nifurtimox and eflornithine [9] as well as the introduction of fexinidazole [10,11], the first oral drug for the treatment of HAT, represent a step forward to an efficacious and safe treatment for this disease. However, drug resistance may still occur, and the existence of animals that represent a reservoir for this infection [12] further justifies research in this area. Amongst the validated parasitic targets, the folate metabolism enzymes represent interesting candidates against trypanosomatidic infections [3]. Trypanosomatidae are auxotrophic for pterins and folates, therefore, inhibiting the enzymes involved in the folate pathways could represent a valuable strategy for the treatment of these trypanosomatidic infections [13,14].

However, although methotrexate (MTX), pyrimethamine (PYR) and trimethoprim (TMP) are nanomolar inhibitors of parasitic dihydrofolate reductase (DHFR) [15], these drugs have reduced activity against *Leishmania* and *Trypanosoma* infections and one of the reasons is the pteridine reductase 1 (PTR1) enzyme. PTR1 is a NADPH-dependent short-chain dehydrogenase/reductase (SDR) mainly involved in the reduction of conjugated and unconjugated pterins, such as biopterin, and in their salvage in the parasitic cells. In *Leishmania*, salvage of extracellular biopterin involves uptake predominantly through the biopterin transporter 1 (BT1) and the fully oxidized pterin is then reduced sequentially to dihydrobiopterin (H_2B) and tetrahydrobiopterin (H_4B) by PTR1 (Figure 1). H_4B is essential for growth of the promastigote stage of *L. major* and it is mainly involved in the biosynthesis

of tyrosine promoted by phenylalanine hydroxylase (PAH) enzyme. PAH enzyme convert H_4B to tetrahydrobiopterine-4a-carbinolamine. The regeneration of H_4B in *L. major* is ensured by two other enzymes: PCD (pteridine carbinolamine dehydrogenase) that convert tetrahydrobiopterine-4a-carbinolamine into quinoide dihydrobiopterin (qH_2B), and qDPR (quinoide dihydropteridine reductase) which finally reduces qH_2B to H_4B (Figure 1). In support of the importance of H_4B for *Leishmania* vitality, there is the evidence that PTR1-null mutants are unable to grow in culture unless supplemented with H_2B or H_4B [14]. In contrast to the leishmania parasites, knockdown of PTR1 levels in *T. brucei* by RNA interference is lethal in vitro and cannot be rescued by supplementation with either H_2B or H_4B [16], unlike *L. major* PTR1-null mutants [17]. In addition, PTR1 knockdown abolishes infectivity of *T. brucei* to mice [16]. These results provide convincing evidence that PTR1 is an essential drug target for the treatment of *T. brucei* infections. Moreover, although PTR1 is mainly involved in the reduction of biopterin to H_4B, it is constitutively involved in the reduction of the 10% of folic acid to tetrahydrofolate required by the parasitic cell, overlapping with the activity of DHFR [14,16]. Thus, when parasitic DHFR is inhibited by antifolate drugs, the expression of PTR1 is increased providing *in toto* the reduced folate necessary for parasite survival, providing a metabolic bypass to alleviate DHFR inhibition and contributing to treatment failure with antifolate drugs [18–21]. Therefore, targeting PTR1, in combination with a classical antifolate drug, is considered a promising strategy for the development of improved therapies [22,23]. Indeed, the combination of PTR1 inhibitors with MTX resulted in a synergic antiparasitic efficacy [24–28]. PTR1 is a functional homo-tetramer having the NADPH cofactor bound in each subunit, stabilized by a tight network of conserved H-bonds [18,29]. The substrate pterin moiety binds in a peculiar π-sandwich between the nicotinamide ring of NADPH and the aromatic side chain of Phe97, suggesting an ordered sequential reaction mechanism relying on the substrate accommodation preceded by the cofactor [18,29].

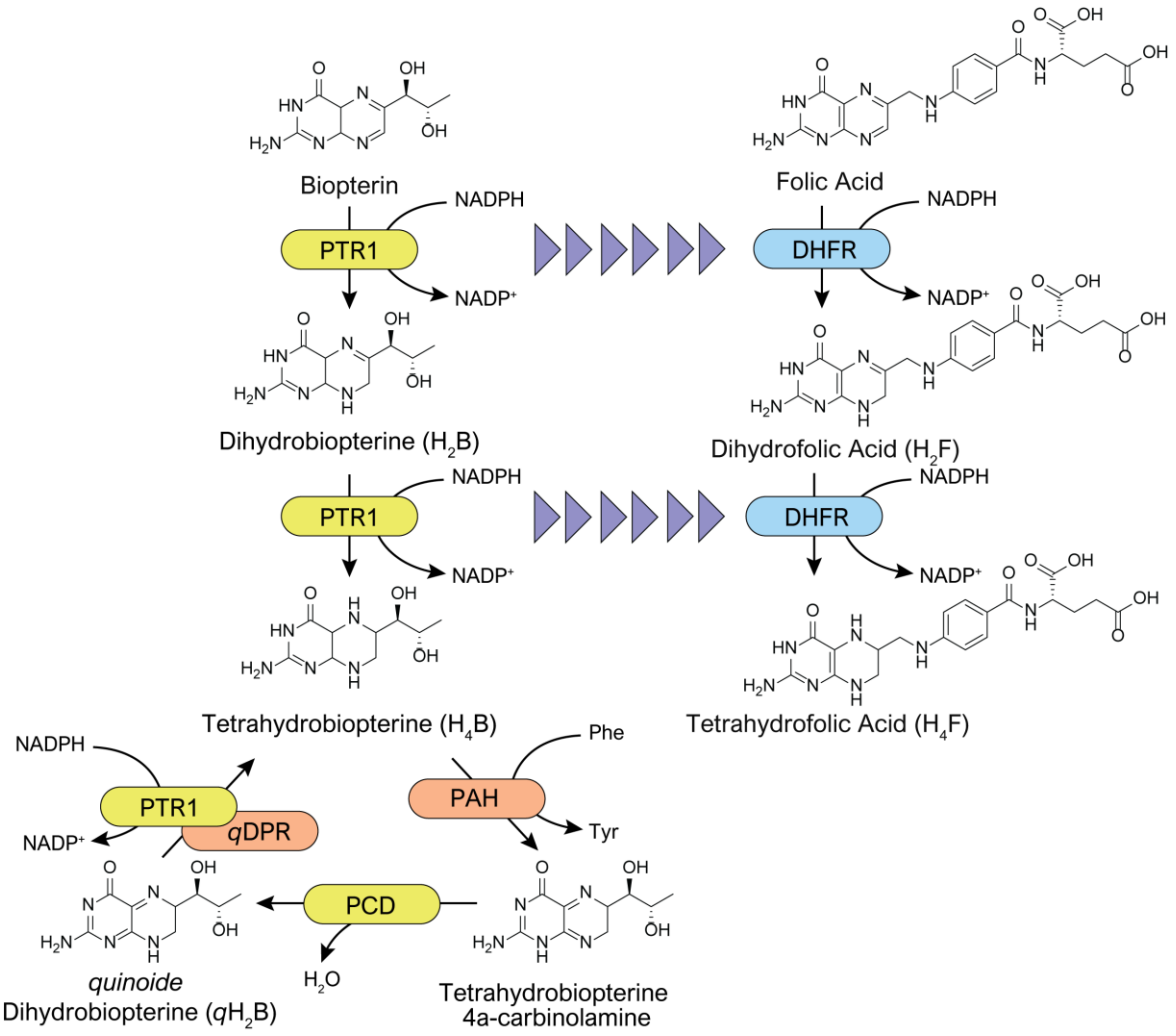

Figure 1. Enzymatic and metabolic pathway of biopterin and folic acid in *T. brucei* and *L. major*.

Almost all PTR1 inhibitors developed to date were designed as competitive inhibitors of biopterin or folic acid, although few non-competitive inhibitors have been recently identified. A wide variety of scaffolds have been explored. However, these possess a substrate-like structure ascribable to the pyrimidine class [18,23,30–32] or to its bioisosteres [25,28,33,34]. Representative chemical scaffolds are reported in **Figure 2**. In order to expand the chemical space and the molecular diversity of the PTR1 inhibitors, several HTS campaigns have been published in the field of trypanosomatidic infections, resulting in a promising array of newly identified hits [35,36]. With this in mind, in the present work, we investigated the utility of the LIBRA compound library (composed of 522 non-commercial molecules contributed by various Italian academic laboratories which have been designed and synthesized during various medicinal chemistry programs) to identify new chemical scaffolds targeting PTR1 as

potential anti-*Trypanosoma* or anti-*Leishmania* agents. The compound library was screened in HTS campaigns against *Trypanosoma brucei* PTR1 (*Tb*PTR1) and *Leishmania major* PTR1 (*Lm*PTR1). The hits identified were assessed for their antiparasitic activity in cell-based parasite assays, both alone and in combination with MTX. The prioritization of compounds was based on their potency in the HTS target-based assays, structural features of each chemotype and physicochemical properties. In addition, we carried out docking studies on the hits identified in the primary screening in order to select only the ones able to bind within the PTR1 binding site and to elucidate their binding mode guiding the design of new derivatives. We ascertained that PTR1 has a preference to bind inhibitors, which resemble its biopterin/folic acid substrates, such as the 2,4-diaminopyrimidine derivatives.

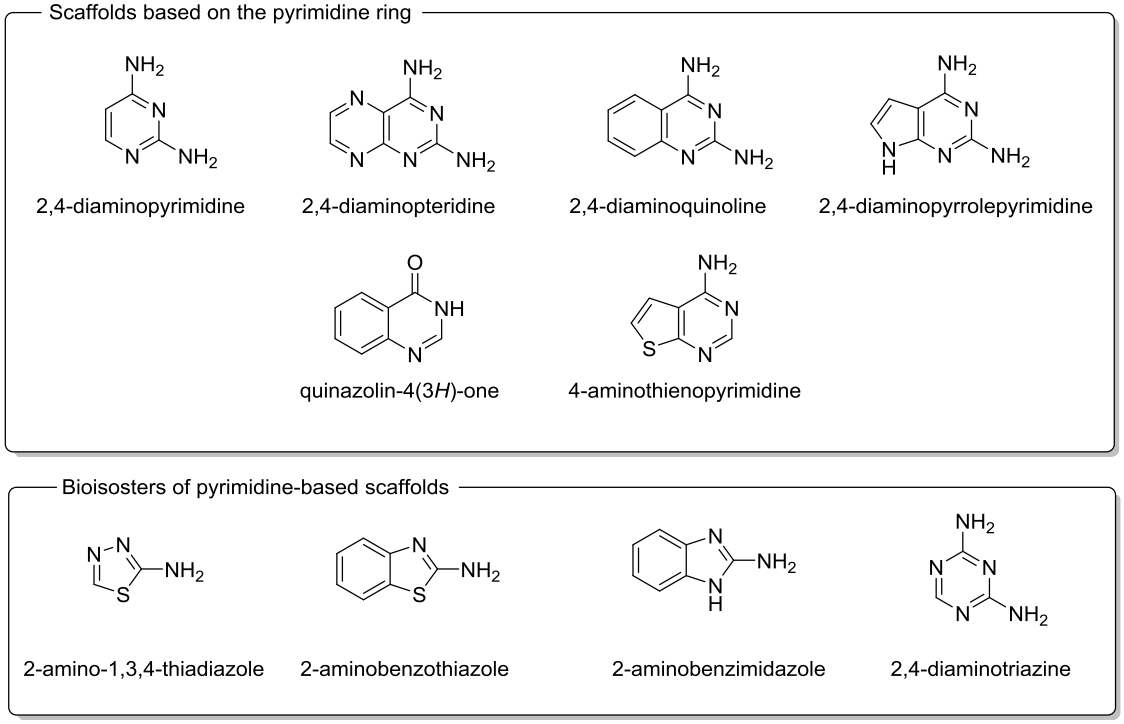

Figure 2. Chemical scaffolds based on the pyrimidine ring or its bioisosteres used for the development of parasitic PTR1 inhibitors.

2. Results and discussion

2.1. LIBRA compound library characterization

The LIBRA compound library consists of 522 non-commercial small molecules synthesized for drug discovery projects in various therapeutic areas (*i.e.* central nervous system [37–39], antitrypanosomal activity [40] and oncology [41]) and donated to the Italian Institute of Technology (IIT) by several Italian academic research groups. Additional details regarding

the main contributors and providers of the compounds forming the LIBRA library are reported in Supporting Information. IIT provided for the assembly and characterization of the library within the LIBRA project. The chemical structures of all the compounds are available as .sdf file which can be downloaded from the LIBRA project website (https://libra-molecules.eu/). The synthesis and characterization of the molecules are reported in the respective publications, which are accessible by searching the chemical structure in SciFinder, the most comprehensive database for chemical literature. The identity of each compound was confirmed using NMR and UPLC-MS and their purity was determined by LC-UV-MS. Compounds that were not detectable in the UV trace (215 nm) or did not ionize by electrospray ionization were analyzed by *q*-NMR. In total, 83% (434 out of 522) and 97% (506 out of 522) of the compounds showed a purity >95% and >85%, respectively (**Table 1**). The identity and purity analyses confirmed the reliability of the tested molecules.

Table 1. Purity of the LIBRA compound library.

Purity (%)	>95%	>90%	>85%	<85%
Number of compounds	434	480	506	16

2.2. Physicochemical properties and chemical space covered by the LIBRA compound library

The chemical space covered by the LIBRA compound library was explored and the most representative chemical scaffolds were identified. For each compound, the extended-connectivity fingerprint 4 (ECFP4) was calculated; the atoms were distinguished by functional type and whether terminal or belonging to a chain or to an aliphatic/aromatic ring; the bonds were distinguished by bond order. A similarity matrix based on the fingerprint was also calculated. When setting the Tanimoto coefficient value at 0.85, a total of 54 chemical clusters were generated. For the molecules of each cluster, the common chemical scaffold was determined and the clusters with the same core scaffold were grouped together. The similarity matrix was also used as an input for the iTOL server (http://itol.embl.de/) [42] to visually represent, as a dendrogram, the chemical similarities between molecules (**Figure 3**). Ten representative chemical clusters were identified: isoxazolines (c1), 1,3-dioxolanes (c4), triazaspiro derivatives (c5), tryptamines (c6), terphenyls (c8), dibenzoannulene (c9), and phenylaminoacetamides (c10). In particular, at least three branches contain a pyrimidine-

based structure, namely c2a (pyrimidines), c2b (purines), and c7 (pyrrolopyrimidones) over the 17 cited core scaffolds.

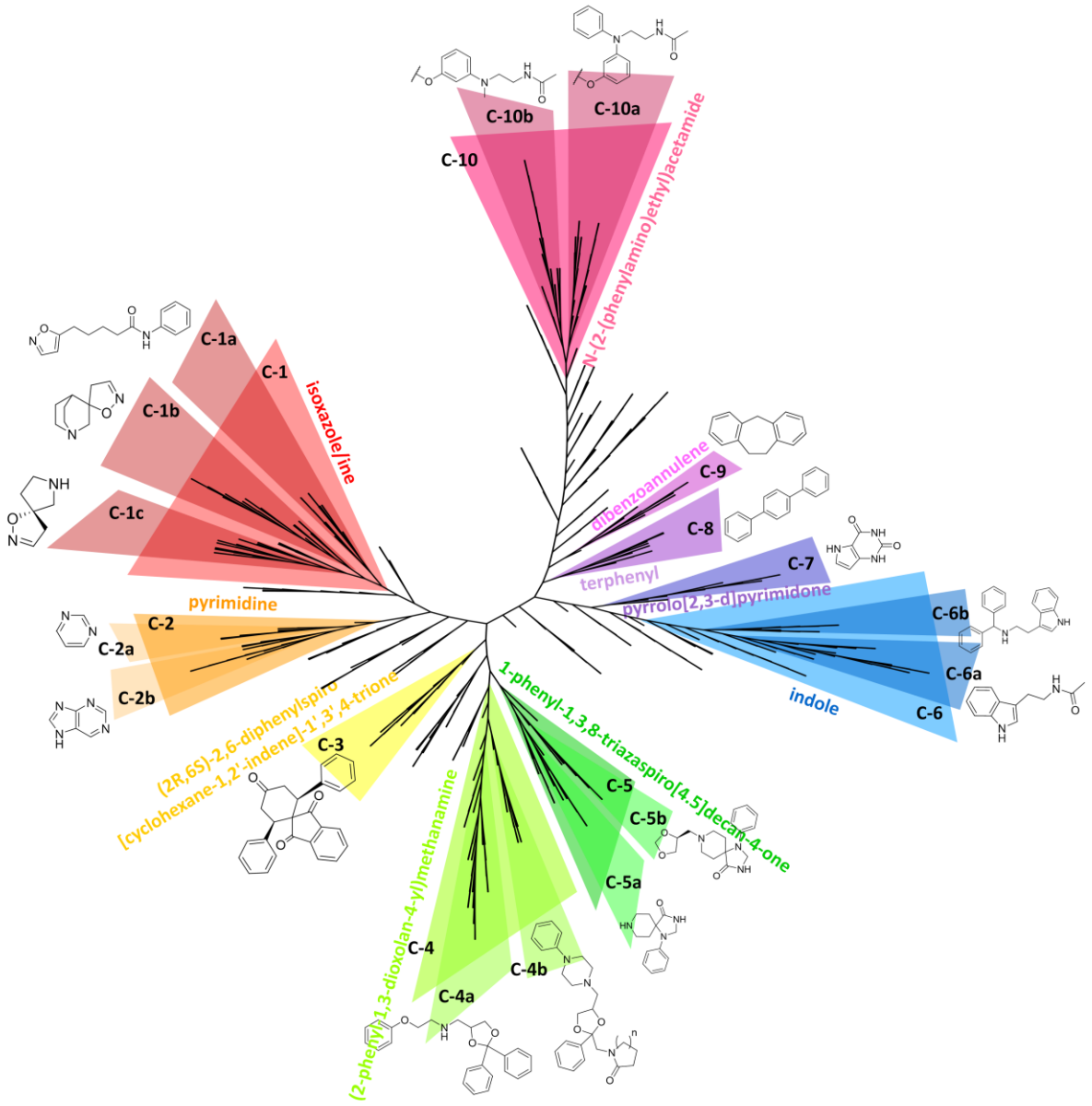

Figure 3. Dendrogram of the LIBRA compound library. Clustering of the library compounds was based on the chemical similarity. Ten clusters were identified; the common chemical scaffold of the compounds of the cluster is reported.

For all 522 LIBRA compounds, the important physiochemical properties and drug-likeness were determined *in silico* and shown to be in accordance with Lipinski's "rule of five (RO5)" [43]. The molecular weight (MW), clog*P*, number of H-bond acceptors (HBA), number of H-bond donors (HBD), total polar surface area (TPSA), and number of rotatable bonds were

calculated using QikProp [44] under the assumption of standard protonation states at physiological pH conditions. These results are summarized in **Table 2**.

Table 2. Physicochemical parameters of the 522 LIBRA compound library.

Parameter	Minimum value	Maximum value	Average	Drug-likeness criteria	% of compounds satisfying the RO5
MW [g/mol]	115	1081	358	<500	89
clog P	-5.62	9.90	2.31	<5	91
H-bond acceptors	1	10	5	<10	100
H-bond donors	0	5	1.2	<5	100
Total polar surface area ($Å^2$)	12	171	60.5	<140	99
Rotatable bonds	0	27	5.1	<10	93
% of compounds passing the RO5 (assuming no more than one violation per compound)					**94.4**

The MW of the compounds ranged between 115 g/mol and 1081 g/mol, with an average of 358 g/mol and a median of 331 g/mol. The calculated lipophilicity (clogP) ranged from −5.62 to 9.90, with a mean value of 2.31. The number of Hydrogen Bond Acceptor (HBA) was 1-10, with an average of 5; whereas the number of Hydrogen Bond Donor (HBD) varied from 0-5, with an average of 1.2. Extending the RO5 evaluation to include properties associated to favourable bioavailability of small molecules [38], the library showed a Total Polar Surface Area (TPSA) ranged 12 $Å^2$-171 $Å^2$, with a mean value of 60.5 $Å^2$, and between 0-27 rotatable bonds, with a mean of 5.1. Assuming no more than one violation of the rule [39], 94.4% of the compounds were in accordance with the RO5. Since the current therapy for HAT is based on drugs administered parentally, except for fexnidazole, all these treatments require a minimum health infrastructure and personnel, not readily available in the remote areas where this pathology is endemic. Therefore, an oral treatment regimen for the disease could potentially allow quicker and wider access to treatment because distribution and administration of tablets is easier. In addition, because over time the disease invades the central nervous system, the candidate drug for HAT should be able to cross the Blood-Brain Barrier (BBB) in order to be effective against the second stage of the diseases. The predictions for human gastrointestinal absorption and BBB permeations are represented in an intuitive graphical classification model viz. BOILED-Egg diagram as shown in **Figure 4**. The 95% of the compounds of the library is predicted to be absorbed per os and the 70% is predicted to be able to cross the BBB, indicating an overall good drug-likeness of the library's components.

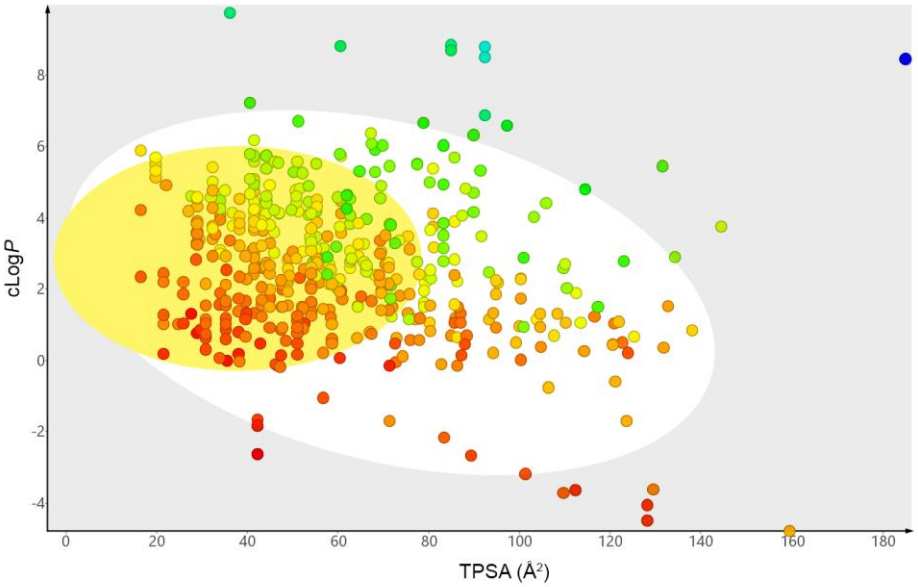

Figure 4. Boiled-egg diagram for the 522 LIBRA compound library. The white region is the physicochemical space of molecules with highest probability of being absorbed by the gastrointestinal tract, and the yellow region (egg yolk) is the physicochemical space of molecules with highest probability to permeate to the brain. The compounds are color-coded by molecular weight (MW) ranging from 115 Da (red dots) to 1081 Da (blue dots).

2.3. HTS campaigns against TbPTR1 and LmPTR1 and hit identification

All 522 compounds of the LIBRA library were initially tested for their inhibitory activity against *Tb*PTR1 and *Lm*PTR1 at 50 µM. The results were reported as a percentage of enzymatic inhibition at 50µM and IC_{50} when appropriate (**Figure 5** and **Table SI-1**). The HTS was performed in duplicate, and the results yielded Z' > 0.9 for all of the assays indicating their high quality. A total of ten compounds (**LIB_66**, **LIB_133**, **LIB_135**, **LIB_136**, **LIB_138**, **LIB_143**, **LIB_146**, **LIB_162**, **LIB_190**, and **LIB_352, Table SI-1**) yielded >85% inhibition at 50µM against *Tb*PTR1 (**Figure 4**, red and green squares). Two compounds were also able to inhibit *Lm*PTR1 >85% (**Figure 4**, green squares), giving an overall hit rate of 1.92% against *Tb*PTR1.

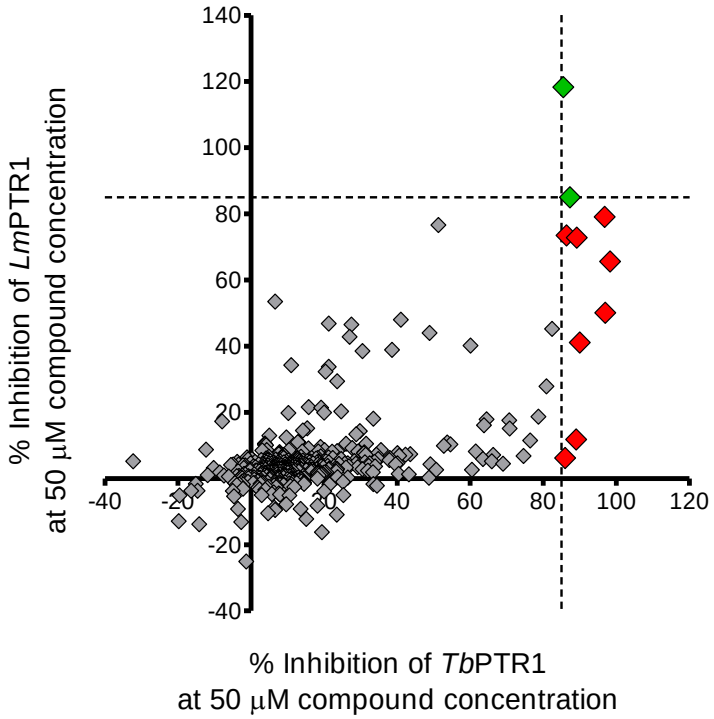

Figure 5. Percentage (%) of inhibition of *Tb*PTR1 and *Lm*PTR1 at 50 μM. The hits selected for the dose-response studies are colored in red (compounds yielding >85% inhibition against *Tb*PTR1) and in green (compounds yielding >85% inhibition against both *Lm*PTR1 and *Tb*PTR1).

The screening hits were tested in nine-point dose response experiments ranging from 0.5 μM to 100 μM, in order to confirm and determine their potencies (IC_{50}). The IC_{50} values were calculated for each compound, which yielded 100% inhibition at the highest compound concentration. Considering the kinetic experiments results and the x-ray crystal structure of **AX5** with TbPTR1, we may conclude that the pyrimidine analogs show a competitive inhibition pattern with respect to the dihydrobiopterine substrate. A similar conclusion was drawn about MTX inhibition pattern. MTX binds into the biopterin binding site preventing the substrate binding and acting as PTR1 competive inhibitor [22]. Compounds **LIB_136** and **LIB_162** (against *Tb*PTR1) and **LIB_66, LIB_135, LIB_136, LIB_146,** and **LIB_190** (against *Lm*PTR1) did not yield 100% inhibition at the highest compound concentration, therefore accurate IC_{50} values were not calculated and are referred to as IC_{50} >100 μM (**Table SI-2**). The Ki for each compound were subsequently calculated assuming a competitive inhibition model [22, 22a] and all data are reported in Table 3. In the dose-response experiments, **LIB_136** yielded no inhibition of PTR1 at a concentration >100 μM, therefore was considered to be a false positive.

Table 3. Compound identifier, chemical structure, and Ki values towards *Tb*PTR1 and *Lm*PTR1 of the nine hits resulting from the HTS campaign.

Compound	Chemical Structure	Compound provider and primary reference[a]	Enzyme inhibition K_i *Tb*PTR1 (μM)	Enzyme inhibition K_i *Lm*PTR1 (μM)
LIB_66	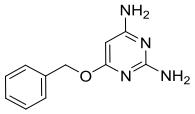	University of Milan Roth, B. et al. [45]	0.6	>100
LIB_133	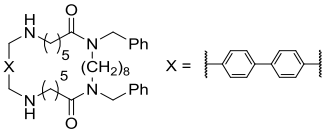	University of Bologna, FaBit Bolognesi, M.L. et al. [46] Rosini, M. et al. [47]	1.6	19.2
LIB_135	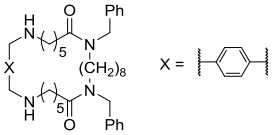	University of Bologna, FaBit Bolognesi, M.L. et al. [46] Rosini, M. et al. [47]	1.7	>100
LIB_138	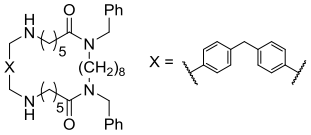	University of Bologna, FaBit Bolognesi, M.L. et al. [46] Rosini, M. et al. [47]	2.7	14.8
LIB_143	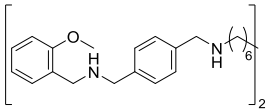	University of Bologna, FaBit Rosini, M. et al. [47]	0.2	37.2
LIB_146	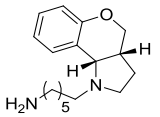	University of Bologna, FaBit Rosini, M. et al. [48]	1.6	>100
LIB_162	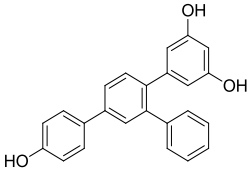	University of Bologna, FaBit Pizzirani, D. et al. [41]	>100	5.7
LIB_190	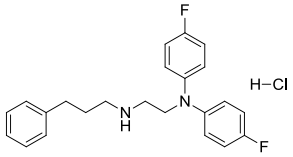	University of Bologna, FaBit Cavalli, A. et al. [49]	2.2	>100
LIB_352	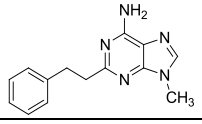	University of Urbino "Carlo Bo" Minetti, P. et al. [50]	4.9	12.0

[a] Bibliographic reference where the synthesis of the compound was reported.
[b] Standard deviation is within ±10% of the value.

Among the nine identified hits from primary screening, eight compounds confirmed the low micromolar activity against *Tb*PTR1 with K_i values ranging from 0.2 to 4.9 uM. In contrast, only five compounds showed measurable K_i against *Lm*PTR1 with values in the 5.7 to 37.2 μM range (Table 3). Basically, the compounds resulted from 2.4 to 167-fold more active against *Tb*PTR1 than *Lm*PTR1, with solely **LIB_352** (*Tb*PTR1 K_i = 4.9 μM and *Lm*PTR1 K_i = 12 μM) showing a comparable activity against both enzymes. The only exception was **LIB_162** that resulted inactive against *Tb*PTR1 but with an K_i = 5.7 μM against LmPTR1.

At this stage, the compounds were solely selected on the basis of their potency, rather than the quality/structural features of each chemotype. Thus, to avoid general promiscuity and toxicity issues associated with a high MW and lipophilicity, compounds with a MW >500 g/mol or cLog*P* >5 were removed [51]. Moreover, the nine compounds resulting from the screening were assessed for pan-assay interference as well as toxicity properties using the *in silico* tool FAFdrugs4 [52,53]. Accordingly, compounds **LIB_133**, **LIB_135**, **LIB_138**, **LIB_143**, and **LIB_146** were discarded due to their high MW, cLogP, number of rigid bonds and ring size. In particular, for compound **LIB_146** the software predicted a high risk associated to the presence of consecutive alkyl chains [54]. **LIB_162** and **LIB_190** presented only low-risk structural alerts due to the presence of a polyphenolic moiety (for **LIB_162**) or polyhalogenated rings (for **LIB_190)** and therefore they were deprioritized. Only **LIB_66** (a diaminopyrimidine, cluster C-2a, **Figure 3**) and **LIB_352** (a purine, cluster C-2b, **Figure 3**) passed the selection criteria. Finally, the two active hits were subjected to a substructure search in literature to identify known chemotypes occurring in approved antiparasitic therapeutics and other published PTR1 inhibitors. To the best of our knowledge, only compound **LIB_66** was chemically close to some *Tb*PTR1 inhibitors reported by Tulloch *et al*. [23] and to a lesser extent to some new *L. chagasi* PTR1 inhibitors discovered by Teixeira *et al.* [31], both based on the 2,4-diaminopyrimidines scaffold. When compared to the previously published compound 4-(benzylthio)-2,6-diaminopyrimidine (**AX5**, **Figure 6A**), **LIB_66** differs from **AX5** by an oxygen atom in place of the sulfur atom in the linker between the pyrimidine and the side benzyl ring [23]. The existence of the active PTR1 inhibitor **AX5** showing a chemical structure similar to **LIB_66** confirmed the accuracy of our processes and suggests that PTR1 has a preference for pyrimidine scaffolds resembling the substrates.

2.4. Docking model of hit compounds with TbPTR1

The availability of a crystallographic structure of **AX5** complexed with *Tb*PTR1 and NADP(H) (PDB ID: 3BMQ) provided the template for a structure-based analysis of the binding of **LIB_66** and **LIB_352** within the catalytic cavity (**Figure 6B**). The 2,6-diaminopyrimidine scaffold of **AX5** binds within the *Tb*PTR1 catalytic pocket forming interactions comparable to those observed between the pteridine moiety of MTX and *Tb*PTR1, in contrast with the canonical pose assumed by the pterin scaffold of the natural PTR1 substrates (*i.e.*, biopterin or folic acid) [23]. The pyrimidine ring is π-π stacked between Phe97 and the nicotinamide ring of NADP(H). The amino group in position 6 is engaged in H-bonding with Tyr174, whereas the second amino group in position 2 establishes a second H-bond with Ser95, anchoring the molecule in the deepest part of the catalytic *Tb*PTR1 active site. The benzylthio side chain in position 4 on the pyrimidine ring of **AX5** is instead located in the hydrophobic pocket of the β6-α6 loop, delimitated by Phe97, Pro210, Trp221, and Met213 (Figure 5B). The binding mode of **LIB_66** and **LIB_352** to the catalytic site of *Tb*PTR1 was investigated by docking studies using Glide [55] and carried out as reported previously on the crystal structure of *Tb*PTR1 (PDB ID: 3JQ7) [21,23]. Docking output revealed that the predicted binding mode of **LIB_66** is in accordance with the crystallographic pose observed for **AX5** (PDB ID: 3BMQ) (**Figure 6C**) [23]. The pyrimidine ring of **LIB_66** stacks in the active site in a π-sandwich between the nicotinamide of $NADP^+$ and Phe97, whereas the phenyl ring establishes a face-to-edge stacking interaction with the aromatic side chain of Trp221 (**Figure 6C**). The H-bonding pattern observed in the *Tb*PTR1-NADP(H)-**AX5** complex was conserved in the predicted binding mode of **LIB_66** (**Figure 6C**). Similarly, the purine ring of **LIB_352** stacks in the active site in a π-sandwich between the nicotinamide of $NADP^+$ and Phe97, with the amino group in position 6 H-bonded to the Tyr174 hydroxyl group (**Figure 6D**). Moreover, the phenyl side chain establishes a face-to-edge stacking interaction with the aromatic side chain of Phe97. However, **LIB_352** was 8-times less active than **LIB_66** (K_i = 4.9 and 0.6 μM, respectively). The slightly reduced activity could be due to the lack of a second amino group to reinforce the binding with $NADP^+$ or Ser95, which is only partially compensated by the stronger π-π interactions established by the extended aromatic system of the purine ring (**Figure 6D**).

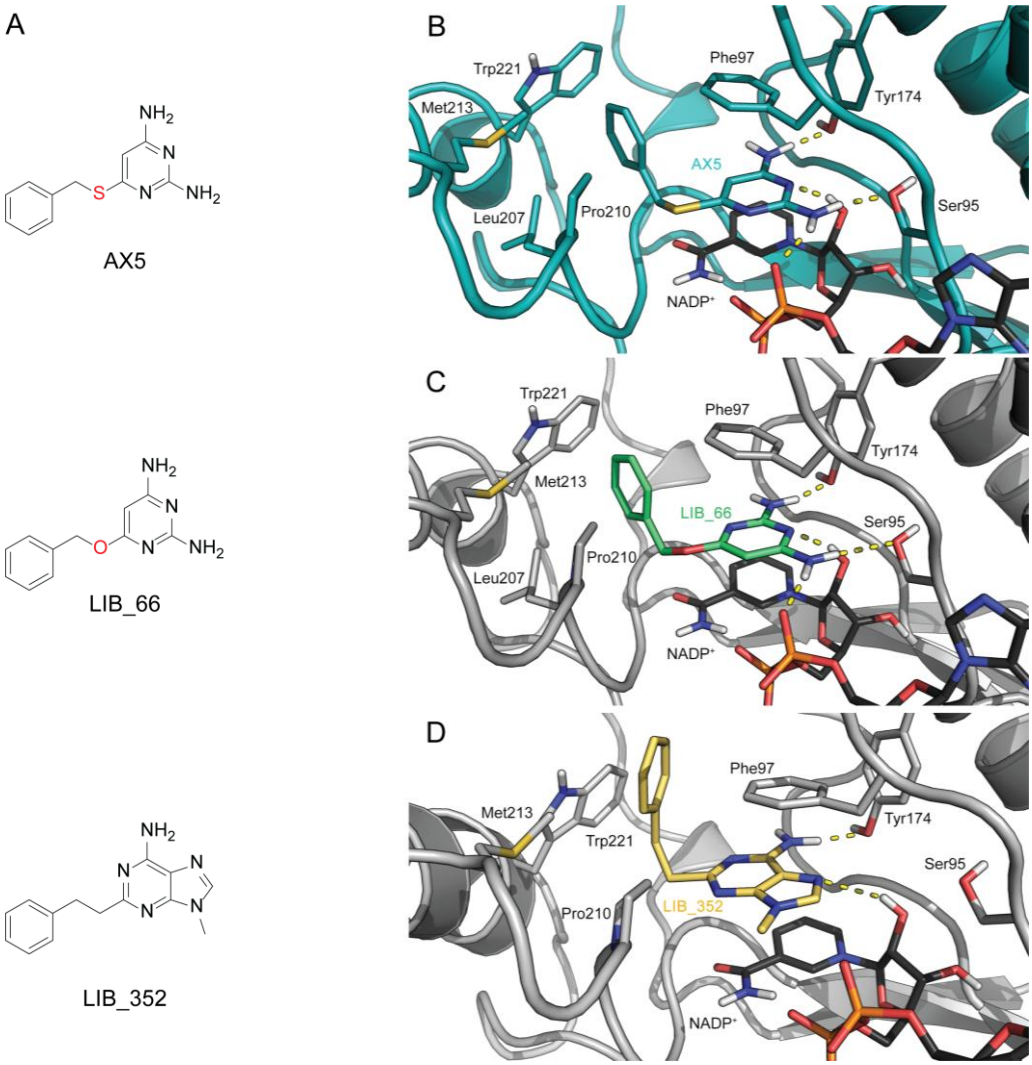

Figure 6. (A) Chemical structures of **AX5**, its bioisostere **LIB_66,** and **LIB_352**. The chemical differences between **LIB_66** and **AX5** are highlighted in red. **(B)** X-ray ternary complex of *Tb*PTR1-NADPH-**AX5** (PDB ID: 3BMQ, **AX5** and protein in teal sticks and cartoon) [23]. **(C)** Docking poses of compound **LIB_66** (sticks, green carbons) in *Tb*PTR1 **(D)** Docking poses of compound **LIB_352** (sticks, yellow carbons) in *Tb*PTR1. The reference crystal structure used for the docking calculation (PDB ID: 2X9G) of *Tb*PTR1 is shown in gray cartoon; important interacting residues are in stick representation with grey carbons, and $NADP^+$ is stick representation in black carbons). Model atoms except for carbons are color-coded with protein carbons (teal or gray), oxygen (red), nitrogen (blue), phosphorous (orange), and sulfur (yellow). H-bonds are represented as dotted lines.

Based on the binding modes observed for *Tb*PTR1, we evaluated possible binding orientations of the selected hits into *Lm*PTR1 by docking calculation that were performed with the same protocol as for *Tb*PTR1. Our results indicated a comparable binding mode between the diaminopyrimidine ring (in **LIB_66**) and the purine ring (in **LIB_352**) with the catalytic pocket of both proteins. *Lm*PTR1 possesses an active site larger than *Tb*PTR1 and with a polar entrance exposed to the solvent (Figure SI-1) [27]. The predicted binding mode

of **LIB_66** indicated that the benzyl is oriented towards the hydrophilic entrance in *Lm*PTR1, therefore it is not able to form π-π stacking or additional hydrophobic contacts (as in *Tb*PTR1). The missing π-π stacking interaction may explain the observed lower activity of **LIB_66** against *Lm*PTR1 (K_i >100 μM) compared with *Tb*PTR1 (K_i : 0.6 μM).

*2.5. **LIB_66** hit confirmation, synthesis, and initial structure-activity relationship (SAR) studies*

Among the two selected hits from the screening, **LIB_66** was the most interesting because of its promising *Tb*PTR1 inhibition (*Tb*PTR1 K_i : 0.6 μM) and its synthetic accessibility that allows rapid structure modification. Therefore, six new **LIB_66** derivatives were prepared and tested *in-vitro* (**Table 4**). These compounds were designed based on visual inspection of the predicted binding mode of **LIB_66** within *Tb*PTR1. First, some substituents were introduced exclusively in the *para* position on the distal benzyl ring in order to capture additional interactions within the two side hydrophobic pockets unique to the *Tb*PTR1 active site (**GC_57, FDS_1, FDS_2,** and **FDS_3**). Second, we replaced the oxygen atom in position 4 of the pyrimidine ring of LIB_66 with a nitrogen to investigate the effect of a hydrogen bond acceptor/donor group at this position. Third, with the aim to confirm the ability of the two amino groups in positions 2 and 6 on the pyrimidine ring to form H-bond contacts with key amino acid residues, the amino group at position 6 was capped with a bulky substituent (**GC_67**).

*2.6. Synthesis of **LIB_66** derivatives*

The synthetic approaches for the new compounds are reported in **Scheme 1**. Compounds **GC_57**, **GC_59**, **GC_67**, and **FDS_1–3** were prepared by aromatic nucleophilic substitution of the appropriate benzyl alcohol or benzyl amine on 4-chloro-2,6-diaminopyrimidine. The reaction conditions were adjusted and optimized for each derivative, allowing the desired compounds to be prepared in >70% yield. **LIB_66** was prepared by reacting commercially available sodium benzyloxide with 4-chloro-2,6-diaminopyrimidine in benzyl alcohol at 150 °C for 5 h. In contrast, for the synthesis of the analogue **GC_57**, the nucleophile was directly generated *in situ* by reacting *p*-methoxybenzyl alcohol with sodium hydride in DMSO, which was to react with 4-chloro-2,6-diaminopyrimidine at a lower temperature (100 °C) for 16 h. The synthesis of the triaminopyrimidine derivatives **GC_67** and **FDS_1–3** required microwave irradiation to afford high yields. The use of one equivalent of the appropriate

benzylamine allowed the mono-benzyl derivative to be selectively obtained, whereas the use of 2.5 equivalents of amine and a longer reaction time (12 h) led to the dibenzyl pyrimidine **GC_67**.

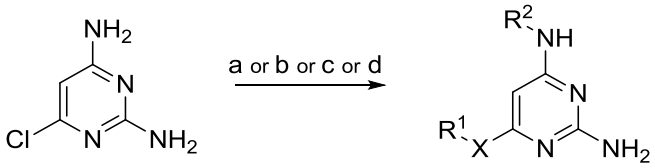

Scheme 1. Reagents and conditions: a) $PhCH_2ONa$, $PhCH_2OH$, 150 °C, 5 h; b) *p*-MeO-$PhCH_2OH$, NaH, DMSO, 100 °C, 16 h; c) R-NH_2 (1 equiv.), EtOH, 150 °C, microwave irradiation, 7 h; d) R-NH_2 (2.5 equiv.), EtOH, 150 °C, microwave irradiation, 12 h.

2.7. PTR1 inhibition and structure-activity relationship (SAR) of the newly synthesized compounds

All six newly synthesized compounds were assessed for the inhibitory activity against *Tb*PTR1. Compounds **GC_57**, **GC_59**, and **FDS_1–3** yielded low micromolar inhibition of *Tb*PTR1 (K_i : 0.2 – 3.4 μM) when compared to that of **LIB_66** (*Tb*PTR1 K_i = 0.6 μM), **FDS_3** being the most potent derivative with K_i of 0.2 μM against *Tb*PTR1 (Table 4). Only compound **GC_67** was completely inactive.

Table 4. Chemical structure, synthetic procedure, and IC_{50} values towards *Tb*PTR1 and *Lm*PTR1 of select compounds.

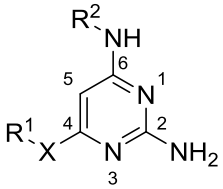

Compound	Chemical Structure				Enzymatic Activity	
	X	R^1	R^2	Synthetic Conditions[a]	K_i *Tb*PTR1 (μM)	K_i *Lm*PTR1 (μM)
LIB_66	O	Bn-	H-	a	0.6±0.1	>100
GC_57	O	(4-MeO)-Bn-	H-	b	0.8±0.1	>100
GC_59	NH	Bn-	H-	c	3.4±1.0	>100
GC_67	NH	Bn-	Bn-	d	N.I.	>100
FDS_1	NH	(4-F)-Bn-	H-	c	1.1±0.1	>100
FDS_2	NH	(4-MeO)-Bn-	H-	c	0.3±0.1	41.6±2.1
FDS_3	NH	(4-Ph)-Bn-	H-	c	0.2±0.1	15.3±1.0

[a] For synthetic procedure and conditions refer to Scheme 1.
[b] Standard deviation is within ±10% of the value unless otherwise specified.
N.I. No inhibition

The inhibition caused by the synthesized compounds and the binding mode predicted by docking calculation allowed to draw a preliminary SAR around the *in-vitro* activity of **LIB_66**. Substitution of the oxygen in position 4 of **LIB_66** with a nitrogen atom, as in **GC_59,** led to a three-fold reduction of inhibitory activity. In contrast, no significative differences in the inhibitor activity were observed when the replacement of the oxygen atom with a nitrogen was applied on the four compounds substituted in position 4 on the side benzyl ring (**GC_57** and **FDS_1–3**). This may be explained by a slightly different binding mode for these four derivatives with respect to the one observed for **LIB_66,** as suggested by computational docking analysis. The introduction of a substituent on the benzyl moiety in **GC_57** and **FDS_1–3** prevents the face-to-edge π interaction between the aromatic ring and Trp221, as observed for **LIB_66**, **GC_59,** and **AX5** (**Figure 6**) [23]. In order to accommodate these substituents, the 2,4-diaminopyrimidine ring, still stacking between Phe97 and nicotinamide, is slightly rotated with respect to **LIB_66**. This torsion allows the phenyl ring of the side chain to establish a face-to-face stacking interaction with the aromatic side chain of Trp221 and a face-to-edge interaction with Phe97 (Figure 6). In addition, for compounds **GC_57** and **FDS_2**, the methoxy group in the *para* position on the distal ring accepts an additional H-bond from Cys168, justifying the slightly higher activity of these two compounds compared with the two analogues without a substituent on the ring (**LIB_66** and **GC_59**, respectively). Compound **FDS_3**, bearing a 4-phenylbenzylamine moiety linked to the 4-position of the pyrimidine scaffold, was the most active compound (*Tb*PTR1 K_i = 0.2 μM). Notably, the biphenyl adopts a substrate-like orientation with the proximal phenyl ring mimicking the *p*-aminobenzoic acid moiety of folic acid and the distal phenyl locking the compound in this orientation by spatial restraints and a face-to-edge interaction with Phe171. Only compound **GC_67** was completely inactive: the introduction of a benzyl group on the nitrogen in position 4 completely prevents the molecule from being accommodated within the *Tb*PTR1 catalytic pocket and blocks the amino group in position 4 to engage an H-bond with Tyr174. In contrast, all the newly synthesized compounds were less active against *Lm*PTR1 than *Tb*PTR1, and the data are in line with the results achieved for the initial hit **LIB_66**. Only compounds **FDS_2** and **FDS_3** showed measurable *Lm*PTR1 K_i of 41.6 and 15.3 μM, respectively .

2.8. Antiparasitic activity towards T. brucei in-vitro

The hits from the screening and the **LIB_66** derivatives, which were active against TbPTR1, were assessed for their antiparasitic activity against the bloodstream form of *T. brucei*. As the compounds yielded modest inhibition of *Lm*PTR1, they were not tested against *Leishmania spp*. The compounds were tested at 10 µM against *T. brucei* in a phenotypic screening campaign with the antiparasitic activity expressed as the percentage of parasitic cell growth inhibition at the defined compound concentration. Compounds with antiparasitic activity >85% at 10 µM were followed up in dose-response studies and six compounds (**LIB_133**, **LIB_135**, **LIB_136**, **LIB_138**, **LIB_143**, and **LIB_190**) yielded EC_{50} against *T. brucei* in the low/sub micromolar range (0.27-6.1 µM). In contrast, two *Tb*PTR1 inhibitors (**LIB_66** and **LIB_352**) and the derivatives of **LIB_66** were inactive against *T. brucei*. Only **FDS_3** showed significant anti-*Trypanosoma* activity as a single agent, with EC_{50} 3.7 µM (**Table 5**).

Table 5. Antiparasitic activity of the hits from the screening and **LIB_66** derivatives against *T. brucei*. EC_{50} of the single compound, antiparasitic activity of the compound in combination with 4 µM MTX and the potentiation index (P.I.) are reported.

	Compound	EC_{50} (µM)	Antiparasitic activity against *T. brucei* % Inhibition + 4 µM MTX[d]	P.I.
Screening hits	**LIB_66**	N.I.	36 ± 3%[b]	1.9 ± 0.1
	LIB_133	0.56 ± 0.04	41 ± 5%[a]	1.2 ± 0.2
	LIB_135	0.61 ± 0.05	43 ± 2%[a]	1.4 ± 0.2
	LIB_138	0.58 ± 0.06	42 ± 2%[a]	1.1 ± 0.1
	LIB_143	0.27 ± 0.03	46 ± 3%[a]	1.1 ± 0.1
	LIB_146	N.I.	51 ± 2%[b]	1.3 ± 0.1
	LIB_190	2.45 ± 0.16	46 ± 4%[a]	1.1 ± 0.2
	LIB_352	N.I.	56 ± 6%[b]	1.7 ± 0.2
Newly synthesized compounds	**GC_57**	N.I.	42 ± 0%[b]	2.2 ± 0.6
	GC_59	N.I.	24 ± 3%[b]	1.3 ± 0.5
	FDS_1	N.I.	37 ± 6%[b]	1.8 ± 0.0
	FDS_2	N.I.	41 ± 6%[b]	2.2 ± 0.6
	FDS_3	3.7 ± 0.8	49 ± 7%[c]	2.3 ± 0.1

N.I.: No inhibition. P.I.: Potentiation Index. [a] Compound screened at 0.1 µM. [b] Compound screened at 10 µM. [c] Compound tested at 1 µM. [d] MTX yielded 19 ± 6 % cell growth inhibition as a single agent at 4 µM.

The effective inhibition of parasite growth was expected when both the PTR1 and DHFR enzymes are inhibited [25,28]. On this basis, we studied the effect of the PTR1 inhibitors in

combination with MTX against *T. brucei* to observe the potentiation effect that the PTR1 inhibitors have on MTX parasite growth inhibition. Thus, eight hits resulting from the screening (**LIB_66**, **LIB_133**, **LIB_135**, **LIB_138**, **LIB_143**, **LIB_146, LIB_190** and **LIB_352**) and the **LIB_66** derivatives were combined with 4 μM MTX (corresponding to the EC_{30} of the DHFR inhibitor against *T. brucei*) [56]. The compounds were assessed in combination at different concentrations, according to their EC_{50} values as a single agent. **LIB_133**, **LIB_135**, **LIB_138**, **LIB_143**, and **LIB_190** were tested at 0.1 μM. **LIB_66**, **LIB_146**, **GC_57**, **GC_59**, **FDS_1**, and **FDS_2** were assessed at 10 μM because they were inactive as single agent. Only compound **FDS_3** was tested at 1 μM since it showed an antiparasitic activity >80% at 10 μM, which is an inhibition potency too high to allow any potentiation effects in combination to be observed. The antiparasitic activity was expressed as the percentage of cell growth inhibition and is reported in **Table 5** and **Figure 7**. The potency in the combination studies was estimated through determination of a potentiating index (P.I.), given by **eq. 1**.

$$P.I. = \frac{\%\ \text{inhibition of the combination}}{(\%\ \text{inhibition of compound} + \%\ \text{inhibition at 4 μM MTX})} \qquad \textbf{eq. 1}$$

A P.I. greater than 1.2 reflects the capacity of the compounds to increase the antiparasitic activity of MTX beyond what would be expected by the simple addition of the individual effects. Except for **LIB_66** and **LIB_352**, the combination of each of the eight compounds from the screening with 4 μM MTX resulted in an additive or partial potentiation activity of MTX (P.I. 1.1-1.4). In contrast, **LIB_352**, **LIB_66** and its derivatives (except for **GC_59**) in combination with 4 μM MTX potentiated the antiparasitic activity of MTX against *T. brucei*, showing P.I. values 1.8-2.3 (**Table 5** and **Figure 7**). This outcome supported the concept that inhibition of both *Tb*PTR1 and *Tb*DHFR is necessary to exert antiparasitic activity *via* the folate pathway.

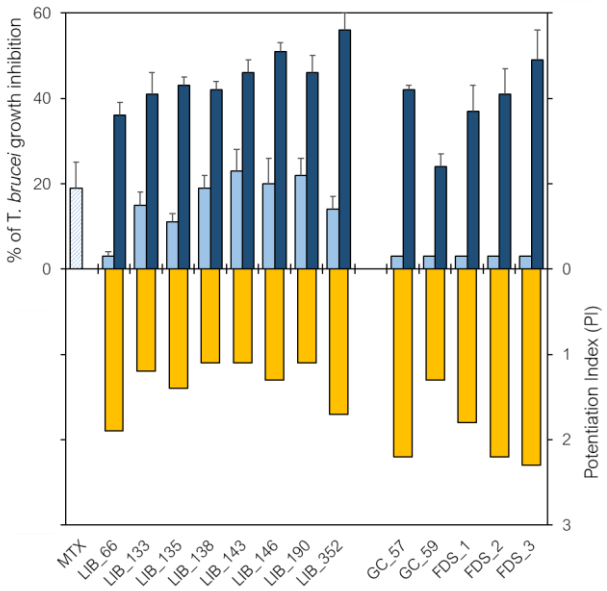

Figure 7. Antiparasitic activity against *T. brucei* of the hits compounds resulting from the screening (**LIB_66**, **LIB_133**, **LIB_135**, **LIB_138**, **LIB_143**, **LIB_146**, **LIB_190** and **LIB_352**) and the **LIB_66** derivatives (**GC_57**, **GC_59**, **FDS_1**, **FDS_2** and **FDS_3**) tested as a single agent (in cerulean) and in combination with 4 μM of MTX (dark blue). Compound **LIB_66**, **LIB_146**, **LIB_352**, **GC_57**, **GC_59**, **FDS_1** and **FDS_2** were tested at 10 μM. Compounds **LIB_133, LIB_135, LIB_138, LIB_143** and **LIB_190** were tested at 0.1 μM. Compound **FDS_3** was tested at 1 μM. The antiparasitic activity of MTX as a single agent at 4 μM is reported in stripped cerulean bar. As a quantitative measure of potentiation, a P.I. of the combination was determined (yellow bar).

2.9. *In vitro early ADMET and selectivity studies against human THP-1 cell lines*

Potential early toxicity-related issues for the **LIB_66** derivatives were determined using early absorption, distribution, metabolism, excretion and toxicity (ADMET) screening technologies. These studies included inhibition of *h*ERG and CYP2D6 as well as mitochondrial toxicity at compound concentration of 10 μM. In addition, the cytotoxicity against two human cell lines, A549 (human lung adenocarcinoma epithelial cells) and THP-1 (human monocytes) were determined. Pentamidine, the first-line drug for the treatment of HAT, was used as reference compound.[57] The cut-off inhibition for each compound tested in the five assays was established for the assessment of a safety profile of the compounds. The results are reported in **Table SI-3** and are organized using a traffic light system for rapid and intuitive visualization (**Figure 8**) The cut-off for acceptable mitochondrial toxicity and inhibition of *h*ERG and CYP2D6 were set at <30% inhibition at 10 μM; whereas for GI_{50} and CC_{50} in the A549 and THP-1 cell-lines, the cut-off was set at >60 μM. With the exception of

the initial hit, namely **LIB_66** which was associated with a safe profile against the five ADMET targets, all six derivatives showed liabilities against *h*ERG (>50% inhibition in the case of **GC_59**, **GC_67**, **FDS_1**, **FDS_2**, and **FDS_3**) and CYP2D6 (30-60% inhibition for **GC_59**, **FDS_1**, and **FDS_2**) and low mitochondrial toxicity was observed. Compound **FDS_3**, besides its promising anti-*T. brucei* activity (EC_{50} of 3.7 µM), showed significant cytotoxicity, with CC_{50} <25 µM against THP-1 cells and GI_{50} of 28.6 µM against A549 cells.

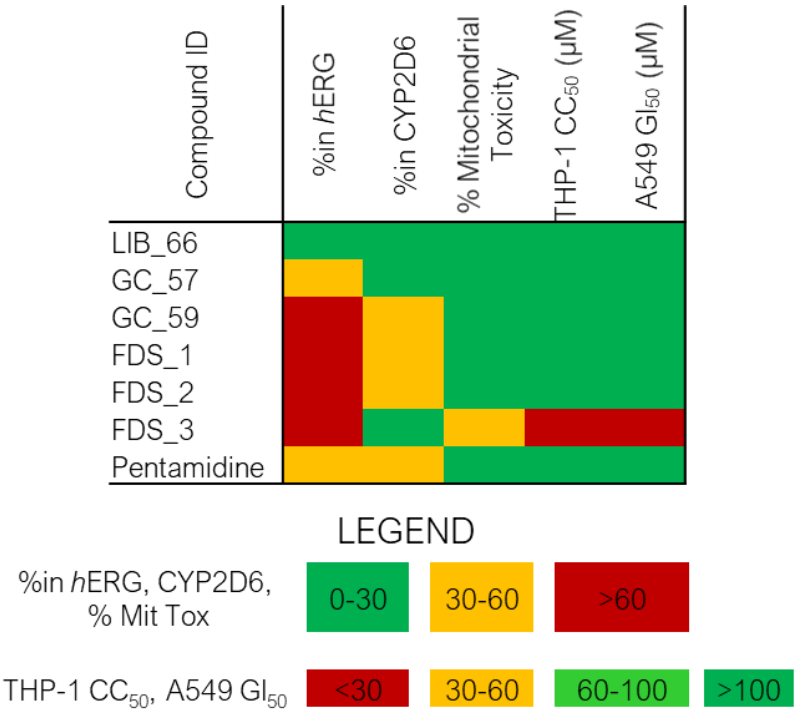

Figure 8. Heat-map data from the *in-vitro* early ADMET assays. Compounds were tested at 10 µM for the *h*ERG, CYP2D6, and mitochondrial toxicity assays. For the THP-1 and A549 cell assays, CC_{50} (<25 µM) and GI_{50} (28.6 µM) were determined for compound FDS_3. Pentamidine was used as reference drug. Red indicates a significant liability, yellow indicates moderate liability and green indicate the absence of liability.

3. Conclusion

In this paper we report the screening of the unique LIBRA compound library against *Tb*PTR1 and *Lm*PTR1 and identified novel compounds, which offer the potential to be progressed as African trypanosomiasis and Leishmaniasis drugs. From the initial screen, **LIB_66**, characterized by a 4-benzyloxy-2,6-diaminopyrimidine structure, was the most interesting hit targeting *Tb*PTR1 (K_i = 0.6 µM). Docking studies indicated that this compound could bind to PTR1 in a similar manner as its natural substrates; the 2,6-diaminopyrimidine scaffold of **LIB_66** displays a binding mode comparable to that of the

pteridine scaffold of MTX, with the benzyloxy side chain in position4 directed towards the hydrophobic pocket, where usually the *p*-aminobenzoic acid ring of folic acid or MTX is located. Hit validation and SAR studies for **LIB_66** were performed by synthesizing a series of 4-(*para*-substituted)benzylamino-2,6-diaminopyrimidine derivatives, in which the pyrimidine scaffold was decorated to explore the biopterin and folic acid binding site. The six compounds showed similar and in some cases improved activity relative to the parent compound, with the SAR rationalized by docking studies. The introduction of a substituent on the benzyl ring induces a slight rotation of the 2,4-diaminopyrimidine ring compared to the reported binding mode of **AX5**. This torsion allows the phenyl ring of the side chain to establish a face-to-face stacking interaction with the aromatic side chain of Trp221 and a face-to-edge interaction with Phe97, whereas the substituents on the benzylic side chain come into contact with the residues forming the distal portion of the *Tb*PTR1 binding pocket, reinforcing binding with the enzyme. Moreover, this different binding mode, induced by the presence of a substituent on the distal aromatic ring, allows the replacement of an H-bond acceptor atom in position 4 (*i.e.*, oxygen or sulfur) with an H-bond donor (*i.e.*, nitrogen), without affecting the activity; these results are in contrast with the preliminary findings observed by Tulloch *et al*. on the smallest 2,4-diaminopyrimidine derivatives [23]. Furthermore, the compounds designed in this study could potentiate *T. brucei* growth inhibition in combination with MTX. These results suggest that the 4-benzyloxy/4-benzylamino-2,6-diaminopyrimidine scaffold can be considered as an interesting starting point for optimization in the drug discovery value chain to search for anti-*T. brucei* agents. The pyrimidine scaffold shows an acceptable ADME-Tox profile as illustrated by **LIB_66** and is suitable for further progression. Amongst the 522 compounds of the LIBRA compound library, which contains at least 17 different chemical scaffolds, PTR1 was inhibited by pyrimidine and purine derivatives, thus confirming the view that PTR1 enzymes prefer substrate-like compounds over other scaffolds. Considering the high need for new and well-characterized chemical entities and for new candidates to be included in the NID pipeline, this work discovered a new opportunity in the field.

4. Materials and Methods

4.1. LIBRA compound library

The compounds are available at the PharmaChemistry Line, Istituto Italiano di Tecnologia, Via Morego 30, I-16163 Genova, Italy. Requests should be addressed to F. Bertozzi:

Fabio.bertozzi@iit.it. Details about LIBRA are reported at the address: https://libra-molecules.eu/.

4.1.1. Characterization of the LIBRA compound library

Compounds (solid or oil) were provided in 1.4 mL barcoded MATRIX microtubes. A weighed aliquot of each compound, enough to make about 1 mL of a 10 mM stock solution, was transferred into another microtube and dissolved with the addition of the proper volume of DMSO-d6. Vigorous shaking ensured dissolution and homogeneity within the microtube. The entire process was automated with a dedicated Hamilton Robotics Microlab Star workstation that also performed transfer of microtube plates in and out of the storage refrigerator, Hamilton Robotics Active Sample Manager, where pure compounds and frozen solutions were stored under nitrogen at 4 °C. The workstation was also capable of detecting partial solubilization; in this case, the solution was manually filtered, and the concentration was determined by quantitative ^{1}H-NMR as described below.

4.1.2. UPLC-MS characterization of the LIBRA compound library

Each compound was submitted to characterization for identity and purity by means of LC-UV-MS. A Waters Acquity instrument equipped with Photodiode Array detector and single quadrupole ESI, equipped with 2.1 x 100 mm UPLC columns (1.7 µm), was used to this purpose. Chromatographic methods and dilution media were adapted to compound polarity, as estimated by cLog*P* as follows. The most polar compounds (cLog*P* <1) were diluted with water/acetonitrile (95/5) and chromatographed on a Waters HSS T3 column with a gradient from 100% to 50% water. Compounds with intermediate polarity (<1 cLog*P* <5) were dissolved in water/acetonitrile (1/1) and chromatographed on a Waters BEH column with a gradient from 90% to 10% water. Less polar compounds (cLog*P* >5) were dissolved in acetonitrile and chromatographed on a Waters BEH column with a gradient from 50% to 0% water. The mobile phase was buffered with 10 mM ammonium acetate, pH 5, and acetonitrile was always used as strong solvent. Flow (0.5 mL/min), gradient duration and column re-equilibration were adapted to UPLC requirements and full method execution did not exceed 10 min per compound. Both positive and negative ion traces were collected and identity was verified for the main chromatographic peak by intense $[M+H]^+$ or $[M+Na]^+$ ions in the positive trace, or $[M-H]^-$ in the negative one. Purity was assessed from the relative main peak

area of the UV trace at 215 nm. Compounds that were not detectable in the 215 nm UV trace or did not ionize in ESI were analyzed by quantitative ^{1}H-NMR.

4.1.3. NMR characterization of the LIBRA compound library

Stock solutions of the compounds in 10 mM DMSO-d6 were submitted to quantitative ^{1}H NMR (*q*-NMR) experiments, which were performed using the PULCON (PUlse Length Based CONcentration Determination) procedure [58]. This procedure does not require the addition of an internal standard as it relies on external standard calibration (performed only once in several months), thus allowing the sample to be used for further analyses (e.g., UPLC-MS) and for biological assays. This method returns both the measured concentration of the compound of interest in solution and its absolute purity by comparison with its theoretical concentration. Structure identities were confirmed by ^{1}H-^{1}H COSY and ^{1}H-^{13}C HSQC experiments. Among the analyzed compounds, the reported structure was confirmed in 81% (138) of cases. Moreover, structure elucidation was performed in more than half of the cases in which the NMR spectra were not in accordance with the reported structure (14 compounds). All the NMR spectra were acquired at 300.0 K on a Bruker Avance III 400 MHz spectrometer equipped with a Broad Band Inverse (BBI) probe. For each compound, 150 µL of 10 mM DMSO-d6 stock solution was transferred into a 3 mm disposable tube (Bruker), which was inserted in the NMR probe using the Sample Jet automatic sampler. Before each acquisition, an automatic matching and tuning were run, and the homogeneity automatically adjusted. In the quantitative ^{1}H-NMR (*q*-NMR) experiments, using the PULCON method, the ^{1}H 90° pulse was optimized on each sample tube by an automatic pulse calculation routine [59]. Then, 16 transients were accumulated over a spectral width of 20.55 ppm (with a transmitter frequency offset at 6.175 ppm), at a fixed receiver gain (64), using 30s of inter-pulses delay and no steady state scans. Spectra were manually phased and automatically baseline corrected. The integrated peaks intensity of the compound under analysis, normalized with respect to proton numbers, was compared to the integrated peak intensity of a 10 mM DMSO-d6 solution of a reference material (maleic acid, Sigma Aldrich NMR standard) whose spectrum was acquired under the same experimental parameters. The PULCON formula returns the measured concentration of the compound under analysis in solution. Absolute (percent) NMR purity was calculated by the ratio between the concentration measured by PULCON and the theoretical concentration (10 mM), multiplied by 100. This is a direct measurement, independent from the detectability of the impurities. 2D experiments for

structure identity or structure elucidation were acquired as follows. ^{1}H-^{1}H COSY (COrrelation SpectroscopY): 4 transients, 2048 data points, 128 increments, with an automatic spectral width and transmitter frequency offset optimization. ^{1}H-^{13}C HSQC (multiplicity edited Heteronuclear Single Quantum Coherence): 8 transients, 1024 data points, 256 increments, with an automatic spectral width and transmitter frequency offset optimization for proton dimension, and with a spectral with of 165.6 ppm and transmitter frequency offsets at 74.6 ppm for carbon dimension.

4.1.4. Determination of kinetic solubility of the LIBRA compound library

The aqueous kinetic solubility (S_{kin}) was determined from a 10 mM DMSO stock solution of test compound in Phosphate Buffered Saline (PBS) at pH 7.4. The study was performed by incubation of an aliquot of 10 mM DMSO stock solution in PBS (pH 7.4) at a target concentration of 250 μM resulting in a final concentration of 2.5% DMSO (v/v). The incubation was carried out under shaking at 25°C for 24 h followed by centrifugation at 14.800 rpm (21100 g) for 30 min. The supernatant was analyzed by UPLC-MS for the quantification of dissolved compound (in μM) by UV at a specific wavelength (215 nm). Compounds were grouped into low (S_{kin} <10 μM), medium/moderate (<10 S_{kin} <100 μM), and high solubility (S_{kin} >100 μM).

4.2. Synthesis

Solvents and chemicals purchased from commercial sources were of analytical grade or better and used without further purification. ^{1}H NMR and ^{13}C NMR spectra were recorded on a Varian Mercury 300 (300 MHz) spectrometer and on a Bruker Avance 400 (400 MHz) spectrometer. Chemical shifts (δ) are expressed in ppm and coupling constants (*J*) are expressed in Hz. TLC analyses were performed on commercial silica gel 60 F254 aluminum sheets; spots were further evidenced by spraying with a dilute alkaline potassium permanganate solution. Melting points were determined on a model B 540 Büchi apparatus and are uncorrected. MS analyses were performed on a Varian 320-MS triple quadrupole mass spectrometer with ESI source. HRMS was obtained on a 6520 Accurate-Mass Q-TOF LC/MS. Compound purity was determined by means of UPLC-MS as described for LIBRA compounds library. All the compounds showed a level of purity above 95%. The compounds passed the check for PAINS performed with the *in-silico* tool FAFdrugs4 [52,53].

*4.2.1. 4-Benzyloxy-2,6-diaminopyrimidine (***LIB_66***)*

The synthetic procedure, the spectroscopic data and physicochemical properties are in accordance with literature [60].

*4.2.2. 9-Methyl-2-phenethyl-9H-purin-6-amine (***LIB_352***)*

CF_3SO_3H (0.37 mL, 3.3 mmol) was added dropwise to a solution of dibenzyl-(9-methyl-2-phenethyl-9H-purin-6-yl)amine (143 mg, 0.33 mmol) in anhydrous CH_2Cl_2 (3 mL), under nitrogen at 0 °C. The mixture was refluxed for 6 h, then cooled and diluted with water, basified to pH 10 with 30% NaOH and extracted with CH_2Cl_2. The organic phase was dried over anhydrous Na_2SO_4 and concentrated. The residue was purified by flash chromatography (cyclohexane-ethyl acetate 3:7) to give a yellow solid that was crystallized from ethanol. Yellow solid (33% yield). M.p.= 140-141 °C. ^{1}H NMR ($CDCl_3$, 400 MHz) δ: 7.73 (s, 1H), 7.29-7.19 (m, 5H), 5.84 (br s, 2H), 3.82 (s, 3H), 3.15 (t, 4H, J = 7.0 Hz). ^{13}C NMR (DMSO, 100 MHz) δ: 158.1, 150.9, 144.8, 140.7, 128.9, 128.8, 126.7, 116.8, 36.8, 33.1, 30.5. ESI-HRMS calcd. for $C_{14}H_{16}N_5$ $[M+H]^+$ 254.1406, found 254.1413.

*4.2.3. 4-(4-Methoxy-benzyloxy-)2,6-diamino methoxybenzyloxypyrimidine (***GC-57***)*

72 mg of NaH (60% on mineral oil, 1.3 eq.) were slowly added to a solution of (4-methoxyphenyl)methanol (171 µL, 1.0 eq.) and 4-chloro-2,6-diaminopyrimidine (200 mg, 1.38 mmol) in DMSO (1.0 mL). The reaction mixture was heated at 100 °C for 16 h. After cooling at room temperature, CH_2Cl_2 (20 mL) was added and the mixture was washed with water (2 x 10 mL). The organic layer was dried over anhydrous Na_2SO_4 and concentrated. The crude was purified by flash chromatography (ethyl acetate 100%) to afford **GC_57** as a yellow solid (70% yield). R_f= 0.37 (ethyl acetate 100%). M.p.= 166.2-167.0 °C. ^{1}H-NMR (DMSO-d_6, 300 MHz) δ: 7.30 (d, *J*= 8.7 Hz, 2H), 6.89 (d, *J*= 8.7 Hz, 2H), 5.98 (s, 2H), 5.86 (s, 2H), 5.10 (s, 2H), 5.03 (s, 1H), 3.72 (s, 3H). ^{13}C-NMR (DMSO-d_6, 75 MHz) δ: 170.3, 166.5, 163.3, 159.3, 130.1, 129.9, 114.1, 76.7, 66.1, 55.5. MS (ESI): *m/z* calcd. for $C_{12}H_{14}N_4O_2$: 246.1; found: 246.9 $[M+H]^+$.

4.2.4. General procedure for the synthesis of 4-benzylamino-2,6-diaminopyrimidine derivatives

The appropriate amine (0.5 mmol) was added to a solution of 4-chloro-2,6-diaminopyrimidine (0.5 mmol) in EtOH (1 mL) in a sealed vial and heated by microwave irradiation at 150 °C for

7 h. After cooling at room temperature, the solvent was evaporated under vacuum the crude material was purified by flash chromatography (CH_2Cl_2/MeOH 9:1) to afford the desired compound.

*4.2.4.1. 4-Benzylamino-2,6-diaminopyrimidine (***GC-59***)*

The spectroscopic data and physicochemical properties are in accordance with literature [61].

*4.2.4.2. 4-(4-Fluoro-benzylamino-)2,6-diaminopyrimidine (***FDS_1***)*

White solid (78% yield). R_f= 0.20 (CH_2Cl_2/MeOH 9:1). M.p.= 125.2-127.5 °C. ^{1}H-NMR (DMSO-d_6, 300 MHz) δ: 7.32-7.24 (m, 2H), 7.14-7.04 (m, 2H), 6.56 (t, *J*= 6.1 Hz, 1H), 5.50 (s, 2H), 5.33 (s, 2H), 4.82 (s, 1H), 4.30 (d, *J*= 6.1 Hz, 2H). ^{13}C-NMR (DMSO-d_6, 75 MHz) δ: 164.8, 164.3, 163.3, 161.4 (d, J_{C-F}= 240.4 Hz), 137.5 (d, J_{C-F}= 2.9 Hz), 129.2 (d, J_{C-F}= 8.0 Hz), 115.2 (d, J_{C-F}= 20.5 Hz), 74.7, 43.3. MS (ESI): *m/z* calcd for $C_{11}H_{12}FN_5$: 233.1; found: 234.1 $[M+H]^+$.

*4.2.4.3. 4-(4-Methoxy-benzylamino-)2,6-diaminopyrimidine (***FDS_2***)*

Yellow solid (83% yield). R_f= 0.28 (CH_2Cl_2/MeOH 9:1). M.p.= dec > 128 °C. ^{1}H-NMR (DMSO-d_6, 300 MHz) δ: 7.17 (d, *J*= 8.4 Hz, 2H), 6.84 (d, *J*= 8.4 Hz, 2H), 6.58 (t, *J*= 5.7 Hz, 1H), 5.60 (s, 2H), 5.45 (s, 2H), 4.82 (s, 1H), 4.25 (d, *J*= 5.7 Hz, 2H), 3.70 (s, 3H). ^{13}C-NMR (DMSO-d_6, 75 MHz) δ: 164.3, 164.2, 162.8, 158.4, 133.0, 128.6, 114.0, 74.5, 55.5, 43.5. MS (ESI): *m/z* calcd for $C_{12}H_{15}N_5O$: 245.1; found: 246.2 $[M+H]^+$.

*4.2.4.4. 4-(4-Phenyl-benzylamino-)2,6-diaminopyrimidine (***FDS_3***)*

Yellow solid (75% yield). R_f= 0.30 (CH_2Cl_2/MeOH 9:1). M.p.= dec. > 141 °C. ^{1}H-NMR (DMSO-d_6, 300 MHz) δ: 7.65-7.54 (m, 4H), 7.42 (t, *J*= 7.7 Hz, 2H), 7.37-7.30 (m, 3H), 6.61 (t, *J*= 6.3 Hz, 1H), 5.52 (s, 2H), 5.35 (s, 2H), 4.84 (s, 1H), 4.37 (d, *J*= 6.3 Hz, 2H). ^{13}C-NMR (DMSO-d_6, 75 MHz) δ: 164.8, 164.3, 163.3, 140.6, 140.5, 138.8, 129.3, 127.9, 127.7, 127.0, 126.9, 74.6, 43.7. MS (ESI): *m/z* calcd for $C_{17}H_{17}N_5$: 291.1; found: 292.1 $[M+H]^+$.

*4.2.4.5. 4,6-Benzylamino-2-aminopyrimidine (***GC_67***)*

4- Benzyl amine (2.5 eq. 1.73 mmol) was added to a solution of 4-chloro-2,6-diaminopyrimidine (0.69 mmol) in EtOH (1 mL) in a sealed vial and heated by microwave irradiation at 150 °C for 12 h. After cooling at room temperature, the solvent was evaporated,

and the crude purified by flash chromatography (CH_2Cl_2/MeOH 9:1) to afford **GC_67** as a yellow solid (73% yield). R_f= 0.23 (CH_2Cl_2/MeOH 95:5). M.p.= dec. > 129 °C. ^{1}H-NMR (DMSO-d_6, 300 MHz) δ: 7.31-7.15 (m, 10H), 6.60 (t, *J*= 5.7 Hz, 2H), 5.43 (s, 2H), 4.83 (s, 1H), 4.31 (d, *J*= 5.7 Hz, 4H). ^{13}C-NMR (DMSO-d_6, 75 MHz) δ: 164.1, 163.1, 141.3, 128.6, 127.4, 126.8, 74.0, 44.1. MS (ESI): *m/z* calcd for $C_{18}H_{19}N_5$: 305.2; found: 306.0 $[M+H]^+$.

4.3. Molecular modelling

Docking was performed using Glide and carried out as previously reported [25,27]. X-ray structures were downloaded from the Protein Data Bank (http://www.rcsb.og) and prepared using prepWizard to assig bond orders and add hydrogen atoms. The 3D structures of the compounds were created from SMILE string and optimized with the OPLS_2005 force field using Maestro [62]. Ionization states and tautomers were generated at pH 7.0±0.5 using Epik [63]. Up to eight stereoisomers and one low-energy ring conformation were generated per compound. For *Tb*PTR1 important structural water sites were previously identified and considered conserved [27]. Refinement was carried out with Prime for residues within 5 Å of the ligand. Up to 20 final docking solutions were reported.

4.4. In-vitro biological assays

4.4.1. TbPTR1 and LmPTR1 protein purification, kinetic characterization purification, screening and IC_{50} determination

The *Tb*PTR1 and *Lm*PTR1 proteins were purified as reported previously [23]. The in-vitro coupled enzyme assays for each enzyme have also been reported in the literature and have independently been shown to be suitable for screening purposes [25,27,36,57,64–67]. For each compound IC_{50}, pIC_{50} values and Hill Slope were determined using a 4-parameter logistic fit in the XE module of ActivityBase (IDBS). The K_i for each compound were calculated using a competitive inhibition model ($K_i = IC_{50}/((S/K_m)+1)$) [22a].

4.4.2. Evaluation of activity against T. brucei

The antiparasitic activity of compounds against *T. brucei* bloodstream forms were evaluated using a modified resazurin-based assay previously described in the literature [68]. The antitrypanosomatid effect was evaluated by the determination of the EC_{50} value (concentration required to inhibit growth by 50%) and calculated by nonlinear regression analysis using GraphPad Prism, Version 5.00 for Windows, GraphPad Software, San Diego California USA (www.graphpad.com). For potentiation experiments, the synergy index was

calculated as the ratio between the activity of the combination (activity of the tested compound in the presence of 4 μM MTX) and the added activity of the components of the combination alone (activity of the compounds + activity of 4 μM MTX).

4.5. In-vitro early ADMET assays

4.5.1. hERG inhibition, CYP2D6 inhibition and mitochondrial toxicity

These assays made use of Invitrogen's Predictor *h*ERG fluorescence polarization assay, Promega P450-Glo assay platform and MitoTracker Red chloromethyl-X-rosamine (CMXRos) uptake and high content imaging to monitor compound-mediated mitochondrial toxicity in the 786-O (renal carcinoma) cell-line respectively as previously described [29].

4.5.2. Cytotoxicity against A549 cell line

The assays were performed using the Cell Titer-Glo assay from Promega. The assay detects cellular ATP content with the amount of ATP being directly proportional to the number of cells present. The A549 cell-line was obtained from DSMZ (German Collection of Microorganisms and Cell Cultures, Braunschweig, Germany) and was grown in DMEM with FCS (10% v/v), streptomycin (100 μg/mL), and penicillin G (100 U/mL) [27].

4.5.3. Cytotoxicity against THP-1 macrophages

The cytotoxicity of THP-1-derived macrophages was assessed by the colorimetric (3-(4,5-dimethylthiazol-2-yl)-2,5-diphenyl tetrazolium bromide) assay [27].

ASSOCIATED CONTENT

Supporting Information. Chemical structures of the 522 compounds; Predicted binding mode on *Lm*PTR1; Inhibitory activity of compounds against *Tb*PTR1 and *Lm*PTR1 of the entire LIBRA library; Inhibition of *h*ERG, CYP2D6, mitochondrial toxicity, and cytotoxicity against A549 and THP-1 cell-lines of **LIB_66** and selected analogues.

AUTHOR INFORMATION

Corresponding Authors.

*A.P. University of Milan, Via Celoria 2, 20133 Milan, Italy; *T.B. Istituto Italiano di Tecnologia; *M.P.C. University of Modena and Reggio Emilia, Via Campi 103, 41125, Modena, Italy.

AUTHOR CONTRIBUTIONS

M.P.C. S.F. and T.B. conceived the work and led the experimental design. M.P.C., P.L. and S.G. wrote the first draft paper and all Authors contributed to manuscript writing. M.L.B., A.P, G.P. M.N., P.C., M.R., F.P., F.B. and M.R., performed the synthetic medicinal chemistry. P.L performed statistical, computational, chemionformatic analyses. T.B., A.C. D.P., E.B. and V.R. contributed to the library collection and maintenance. S.G., G.W, M.K. and B.E, performed the early ADMET assays. A.C. and N.S. performed the anti-parasitic assays. The authors declare no competing financial interest.

Present Addresses

[†]Department of Biomedicine, University of Basel, Mattenstrasse 28, 4058 Basel, Switzerland.

ACKNOWLEDGMENT

This project has received funding from the European Union's Seventh Framework Programme for research, technological development and demonstration under grant agreement n° 603240 (NMTrypI - New Medicines for Trypanosomatidic Infections). We thank Silvia Venzano for handling of the Libra compound collection, and Anna Maddalena and Mattia Pini for support in data storage.

ABBREVIATIONS

ADMET, absorption, distribution, metabolism, excretion and toxicity; CYP, cytochrome P450; DHFR, dihydrofolate reductase; *Leishmania* spp., Leishmania specie; *L. infantum*, *Leishmania infantum*; *L. major*, *Leishmania major*; *Lm*PTR1, *Leishmania major* pteridine reductase-1; MTX, methotrexate; P.I., Potentiating Index; PTR1, pteridine reductase-1; *Tb*PTR1, *Trypanosoma brucei* pteridine reductase-1; *T. brucei* or *Tb*, *Trypanosoma brucei*.

REFERENCES

[1] A. Roy, P.R. McDonald, S. Sittampalam, R. Chaguturu, Open Access High Throughput Drug Discovery in the Public Domain: A Mount Everest in the Making, Curr. Pharm. Biotechnol. 11 (2010) 764–778. http://www.ncbi.nlm.nih.gov/pmc/articles/PMC3716285/.

[2] J. Baell, M.A. Walters, Chemistry: Chemical con artists foil drug discovery, Nature. 513 (2014) 481–483. doi:10.1038/513481a.

[3] I.H. Gilbert, Drug Discovery for Neglected Diseases: Molecular Target-Based and Phenotypic Approaches: Miniperspectives Series on Phenotypic Screening for Antiinfective Targets, J. Med. Chem. 56 (2013) 7719–7726. doi:10.1021/jm400362b.

[4] K. Nussbaum, J. Honek, C.M.C. v C. Cadmus, T. Efferth, Trypanosomatid parasites causing neglected diseases., Curr. Med. Chem. 17 (2010) 1594–1617.

[5] K.R. Matthews, The developmental cell biology of Trypanosoma brucei., J. Cell Sci. 118 (2005) 283–290. doi:10.1242/jcs.01649.

[6] A. Machado-Silva, P.P.G. Guimaraes, C.A.P. Tavares, R.D. Sinisterra, New perspectives for leishmaniasis chemotherapy over current anti-leishmanial drugs: a patent landscape., Expert Opin. Ther. Pat. 25 (2015) 247–260. doi:10.1517/13543776.2014.993969.

[7] E. Chatelain, J.-R. Ioset, Drug discovery and development for neglected diseases: the DNDi model, Drug Des. Devel. Ther. 5 (2011) 175–181. doi:10.2147/DDDT.S16381.

[8] M.P. Barrett, I.M. Vincent, R.J.S. Burchmore, A.J.N. Kazibwe, E. Matovu, Drug resistance in human African trypanosomiasis., Future Microbiol. 6 (2011) 1037–1047. doi:10.2217/fmb.11.88.

[9] E. Alirol, D. Schrumpf, J. Amici Heradi, A. Riedel, C. De Patoul, M. Quere, F. Chappuis, Nifurtimox-eflornithine combination therapy for second-stage gambiense human African trypanosomiasis: Médecins Sans Frontières experience in the Democratic Republic of the Congo, Clin. Infect. Dis. 56 (2013) 195–203. doi:10.1093/cid/cis886.

[10] A. Maxmen, Pill treats sleeping sickness Scientists seek approval from regulators for this relatively quick and easy therapy ., Nature. 550 (2017) 441.

[11] E. Torreele, B.B. Trunz, D. Tweats, M. Kaiser, R. Brun, G. Mazué, M.A. Bray, B. Pécoul, Fexinidazole - a new oral nitroimidazole drug candidate entering clinical development for the treatment of sleeping sickness, PLoS Negl. Trop. Dis. 4 (2010) 1–15. doi:10.1371/journal.pntd.0000923.

[12] M.K. N'Djetchi, H. Ilboudo, M. Koffi, J. Kaboré, J.W. Kaboré, D. Kaba, F. Courtin, B. Coulibaly, P. Fauret, L. Kouakou, S. Ravel, S. Deborggraeve, P. Solano, T. De Meeûs, B. Bucheton, V. Jamonneau, The study of trypanosome species circulating in domestic animals in two human African trypanosomiasis foci of Côte d'Ivoire identifies pigs and cattle as potential reservoirs of Trypanosoma brucei gambiense, PLoS Negl. Trop. Dis. 11 (2017) e0005993. https://doi.org/10.1371/journal.pntd.0005993.

[13] B. Nare, L.W. Hardy, S.M. Beverley, The roles of pteridine reductase 1 and dihydrofolate reductase- thymidylate synthase in pteridine metabolism in the protozoan parasite Leishmania major, J. Biol. Chem. 272 (1997) 13883–13891. doi:10.1074/jbc.272.21.13883.

[14] a R. Bello, B. Nare, D. Freedman, L. Hardy, S.M. Beverley, PTR1: a reductase mediating salvage of oxidized pteridines and methotrexate resistance in the protozoan parasite Leishmania major., Proc. Natl. Acad. Sci. U. S. A. 91 (1994) 11442–11446. doi:10.1073/pnas.91.24.11442.

[15] I.H. Gilbert, Inhibitors of dihydrofolate reductase in Leishmania and trypanosomes., Biochim. Biophys. Acta. 1587 (2002) 249–257.

[16] N. Sienkiewicz, H.B. Ong, A.H. Fairlamb, Trypanosoma brucei pteridine reductase 1 is essential for survival in vitro and for virulence in mice, Mol. Microbiol. 77 (2010) 658–671. doi:10.1111/j.1365-2958.2010.07236.x.

[17] M.L. Cunningham, S.M. Beverley, Pteridine salvage throughout the Leishmania infectious cycle: Implications for antifolate chemotherapy, Mol. Biochem. Parasitol. 113 (2001) 199–213. doi:10.1016/S0166-6851(01)00213-4.

[18] A. Dawson, F. Gibellini, N. Sienkiewicz, L.B. Tulloch, P.K. Fyfe, K. McLuskey, A.H. Fairlamb, W.N. Hunter, Structure and reactivity of Trypanosoma brucei pteridine reductase: Inhibition by the archetypal antifolate methotrexate, Mol. Microbiol. 61 (2006) 1457–1468. doi:10.1111/j.1365-2958.2006.05332.x.

[19] D. Guerrieri, S. Ferrari, M.P. Costi, P.A.M. Michels, Biochemical effects of riluzole on Leishmania parasites, Exp. Parasitol. 133 (2013) 250–254. doi:10.1016/j.exppara.2012.11.013.

[20] K.L. Barrack, L.B. Tulloch, L.A. Burke, P.K. Fyfe, W.N. Hunter, Structure of recombinant Leishmania donovani pteridine reductase reveals a disordered active site, Acta Crystallogr. Sect. F Struct. Biol. Cryst. Commun. 67 (2011) 33–37. doi:10.1107/S174430911004724X.

[21] S. Ferrari, F. Morandi, D. Motiejunas, E. Nerini, S. Henrich, R. Luciani, A. Venturelli, S. Lazzari, S. Calò, S. Gupta, V. Hannaert, P.A.M. Michels, R.C. Wade, M.P. Costi, Virtual screening identification of nonfolate compounds, including a CNS drug, as antiparasitic agents inhibiting pteridine reductase, J. Med. Chem. 54 (2011) 211–221. doi:10.1021/jm1010572.

[22] A. Cavazzuti, G. Paglietti, W.N. Hunter, F. Gamarro, S. Piras, M. Loriga, S. Allecca, P.

Corona, K. McLuskey, L. Tulloch, F. Gibellini, S. Ferrari, M.P. Costi, Discovery of potent pteridine reductase inhibitors to guide antiparasite drug development., Proc. Natl. Acad. Sci. U. S. A. 105 (2008) 1448–1453. doi:10.1073/pnas.0704384105. 22a Segel, I.H. (1993) Enzyme kinetics: Behavior and analysis of rapid equilibrium and steady-state enzyme systems. John Wiley & Sons, Inc., New York.

[23] L.B. Tulloch, V.P. Martini, J. Iulek, J.K. Huggan, J.H. Lee, C.L. Gibson, T.K. Smith, C.J. Suckling, W.N. Hunter, Structure-based design of pteridine reductase inhibitors targeting African sleeping sickness and the leishmaniases., J. Med. Chem. 53 (2010) 221–229. doi:10.1021/jm901059x.

[24] P. Linciano, C.B. Moraes, L.M. Alcantara, C.H. Franco, B. Pascoalino, L.H. Freitas-Junior, S. Macedo, N. Santarem, A. Cordeiro-da-Silva, S. Gul, G. Witt, M. Kuzikov, B. Ellinger, S. Ferrari, R. Luciani, A. Quotadamo, L. Costantino, M.P. Costi, Aryl thiosemicarbazones for the treatment of trypanosomatidic infections, Eur. J. Med. Chem. 146 (2018) 423–434. doi:10.1016/j.ejmech.2018.01.043.

[25] P. Linciano, A. Dawson, I. Pöhner, D.M. Costa, M.S. Sá, A. Cordeiro-da-Silva, R. Luciani, S. Gul, G. Witt, B. Ellinger, M. Kuzikov, P. Gribbon, J. Reinshagen, M. Wolf, B. Behrens, V. Hannaert, P.A.M. Michels, E. Nerini, C. Pozzi, F. di Pisa, G. Landi, N. Santarem, S. Ferrari, P. Saxena, S. Lazzari, G. Cannazza, L.H. Freitas-Junior, C.B. Moraes, B.S. Pascoalino, L.M. Alcântara, C.P. Bertolacini, V. Fontana, U. Wittig, W. Müller, R.C. Wade, W.N. Hunter, S. Mangani, L. Costantino, M.P. Costi, Exploiting the 2-Amino-1,3,4-thiadiazole Scaffold To Inhibit *Trypanosoma brucei* Pteridine Reductase in Support of Early-Stage Drug Discovery, ACS Omega. 2 (2017) 5666–5683. doi:10.1021/acsomega.7b00473.

[26] C. Borsari, N. Santarem, J. Torrado, A. Isabel, M. Jesús, C. Baptista, S. Gul, M. Wolf, M. Kuzikov, B. Ellinger, G. Witt, P. Gribbon, J. Reinshagen, P. Linciano, A. Tait, L. Costantino, L.H. Freitas-junior, C.B. Moraes, P. Bruno, L. Maria, C.H. Franco, C.D. Bertolacini, V. Fontana, P. Tejera, J. Clos, A. Cordeiro-da-silva, S. Ferrari, M. Paola, Methoxylated 2 ’ -hydroxychalcones as antiparasitic hit compounds, Eur. J. Med. Chem. 126 (2017) 1129–1135. doi:10.1016/j.ejmech.2016.12.017.

[27] C. Borsari, R. Lucian, C. Pozz, I. Poehner, S. Henrich, M. Trande, A. Cordeiro-Da-silva, N. Santarem, C. Baptista, A. Tait, F. Di Pisa, L. Dello Iacono, G. Landi, S. Gul, M. Wolf, M. Kuzikov, B. Ellinger, J. Reinshagen, G. Witt, P. Gribbon, M. Kohler, O. Keminer, B. Behrens, L. Costantino, P.T. Nevado, E. Bifeld, J. Eick, J. Clos, J.

Torrado, M.D. Jim??nez-Ant??n, M.J. Corral, J.M. Alunda, F. Pellati, R.C. Wade, S. Ferrari, S. Mangani, M.P. Costi, Profiling of flavonol derivatives for the development of antitrypanosomatidic drugs, J. Med. Chem. 59 (2016) 7598–7616. doi:10.1021/acs.jmedchem.6b00698.

[28] P. Linciano, C. Pozzi, L. Dello Iacono, F. di PIsa, G. Landi, A. Bonucci, S. Gul, M. Kuzikov, B. Ellinger, G. Witt, N. Santarem, C. Baptista, C. Franco, C. Borsoi Moraes, W. Müller, U. Wittig, R. Luciani, A. Sesenna, A. Quotadamo, S. Ferrari, I. Pöhner, A. Cordeiro-da-Silva, S. Mangani, L. Costantino, M.P. Costi, Enhancement of benzothiazoles as Pteridine Reductase-1 (PTR1) inhibitors for the treatment of Trypanosomatidic infections., J. Med. Chem. (2019). doi:10.1021/acs.jmedchem.8b02021.

[29] D.G. Gourley, a W. Schüttelkopf, G. a Leonard, J. Luba, L.W. Hardy, S.M. Beverley, W.N. Hunter, Pteridine reductase mechanism correlates pterin metabolism with drug resistance in trypanosomatid parasites., Nat. Struct. Biol. 8 (2001) 521–525. doi:10.1038/88584.

[30] A. Dawson, L.B. Tulloch, K.L. Barrack, W.N. Hunter, High-resolution structures of Trypanosoma brucei pteridine reductase ligand complexes inform on the placement of new molecular entities in the active site of a potential drug target, Acta Crystallogr. Sect. D Biol. Crystallogr. 66 (2010) 1334–1340. doi:10.1107/S0907444910040886.

[31] B.V.F. Teixeira, A.L.B. Teles, S.G. da Silva, C.C.B. Brito, H.F. de Freitas, A.B.L. Pires, T.Q. Froes, M.S. Castilho, Dual and selective inhibitors of pteridine reductase 1 (PTR1) and dihydrofolate reductase-thymidylate synthase (DHFR-TS) from Leishmania chagasi , J. Enzyme Inhib. Med. Chem. 34 (2019) 1439–1450. doi:10.1080/14756366.2019.1651311.

[32] F.H.A. Leite, T.Q. Froes, S.G. da Silva, E.I.M. de Souza, D.G. Vital-Fujii, G.H.G. Trossini, S.S. da R. Pita, M.S. Castilho, An integrated approach towards the discovery of novel non-nucleoside Leishmania major pteridine reductase 1 inhibitors, Eur. J. Med. Chem. 132 (2017) 322–332. doi:10.1016/j.ejmech.2017.03.043.

[33] D. Spinks, H.B. Ong, C.P. Mpamhanga, E.J. Shanks, D.A. Robinson, I.T. Collie, K.D. Read, J.A. Frearson, P.G. Wyatt, R. Brenk, A.H. Fairlamb, I.H. Gilbert, Design, synthesis and biological evaluation of novel inhibitors of Trypanosoma brucei pteridine reductase 1., ChemMedChem. 6 (2011) 302–8. doi:10.1002/cmdc.201000450.

[34] G. Landi, P. Linciano, C. Borsari, C.P. Bertolacini, C.B. Moraes, A. Cordeiro-da-Silva,

S. Gul, G. Witt, M. Kuzikov, M.P. Costi, C. Pozzi, S. Mangani, Structural Insights into the Development of Cycloguanil Derivatives as Trypanosoma brucei Pteridine-Reductase-1 Inhibitors, ACS Infect. Dis. (2019) ahead of print. doi:10.1021/acsinfecdis.8b00358.

[35] M.C. Field, D. Horn, A.H. Fairlamb, M.A.J. Ferguson, D.W. Gray, K.D. Read, M. De Rycker, L.S. Torrie, P.G. Wyatt, S. Wyllie, I.H. Gilbert, Anti-trypanosomatid drug discovery: an ongoing challenge and a continuing need., Nat. Rev. Microbiol. 15 (2017) 217–231. doi:10.1038/nrmicro.2016.193.

[36] C.B. Moraes, G. Witt, M. Kuzikov, B. Ellinger, T. Calogeropoulou, K.C. Prousis, S. Mangani, F. Di Pisa, G. Landi, L. Dello Iacono, C. Pozzi, L.H. Freitas-Junior, B. dos Santos Pascoalino, C.P. Bertolacini, B. Behrens, O. Keminer, J. Leu, M. Wolf, J. Reinshagen, A. Cordeiro-da-Silva, N. Santarem, A. Venturelli, S. Wrigley, D. Karunakaran, B. Kebede, I. Pöhner, W. Müller, J. Panecka-Hofman, R.C. Wade, M. Fenske, J. Clos, J.M. Alunda, M.J. Corral, E. Uliassi, M.L. Bolognesi, P. Linciano, A. Quotadamo, S. Ferrari, M. Santucci, C. Borsari, M.P. Costi, S. Gul, Accelerating Drug Discovery Efforts for Trypanosomatidic Infections Using an Integrated Transnational Academic Drug Discovery Platform, SLAS Discov. Adv. Life Sci. R&D. 24 (2019) 346–361. doi:10.1177/2472555218823171.

[37] A. Prandi, S. Franchini, L.I. Manasieva, P. Fossa, E. Cichero, G. Marucci, M. Buccioni, A. Cilia, L. Pirona, L. Brasili, Synthesis, Biological Evaluation, and Docking Studies of Tetrahydrofuran- Cyclopentanone- and Cyclopentanol-Based Ligands Acting at Adrenergic α1- and Serotonine 5-HT1A Receptors, J. Med. Chem. 55 (2012) 23–36. doi:10.1021/jm200421e.

[38] M.L. Bolognesi, M. Bartolini, A. Cavalli, V. Andrisano, M. Rosini, A. Minarini, C. Melchiorre, Design, Synthesis, and Biological Evaluation of Conformationally Restricted Rivastigmine Analogues, J. Med. Chem. 47 (2004) 5945–5952. doi:10.1021/jm049782n.

[39] C. Dallanoce, P. Bazza, G. Grazioso, M. De Amici, C. Gotti, L. Riganti, F. Clementi, C. De Micheli, Synthesis of epibatidine-related Δ2-isoxazoline derivatives and evaluation of their binding affinity at neuronal nicotinic acetylcholine receptors, European J. Org. Chem. (2006) 3746–3754. doi:10.1002/ejoc.200600231.

[40] P. Conti, A. Pinto, P.E. Wong, L.L. Major, L. Tamborini, M.C. Iannuzzi, C. De Micheli, M.P. Barrett, T.K. Smith, Synthesis and in vitro/in vivo evaluation of the

antitrypanosomal activity of 3-bromoacivicin, a potent CTP synthetase inhibitor., ChemMedChem. 6 (2011) 329–333. doi:10.1002/cmdc.201000417.

[41] D. Pizzirani, M. Roberti, A. Cavalli, S. Grimaudo, A. Di Cristina, R.M. Pipitone, N. Gebbia, M. Tolomeo, M. Recanatini, Antiproliferative agents that interfere with the cell cycle at the G1-->S transition: further development and characterization of a small library of stilbene-derived compounds., ChemMedChem. 3 (2008) 345–355. doi:10.1002/cmdc.200700258.

[42] I. Letunic, P. Bork, Interactive tree of life (iTOL) v3: an online tool for the display and annotation of phylogenetic and other trees., Nucleic Acids Res. 44 (2016) W242-5. doi:10.1093/nar/gkw290.

[43] C.A. Lipinski, Drug-like properties and the causes of poor solubility and poor permeability, J. Pharmacol. Toxicol. Methods. 44 (2000) 235–249. doi:10.1016/S1056-8719(00)00107-6.

[44] L. Schrödinger, Schrödinger Release 2017-1: QikProp, (2017).

[45] B. Roth, J.M. Smith, M.E. Hultquist, Analogs of Pteroylglutamic Acid. VIII. 4-Alkoxy Derivatives, J. Am. Chem. Soc. 73 (1951) 2869–2871. doi:10.1021/ja01150a131.

[46] M.L. Bolognesi, M.G. Bixel, G. Marucci, M. Bartolini, M. Krauss, P. Angeli, A. Antonello, M. Rosini, V. Tumiatti, F. Hucho, C. Melchiorre, Structure-activity relationships of methoctramine-related polyamines as muscular nicotinic receptor noncompetitive antagonists. 3. Effect of inserting the tetraamine backbone into a macrocyclic structure., J. Med. Chem. 45 (2002) 3286–3295.

[47] M. Rosini, M.G. Bixel, G. Marucci, R. Budriesi, M. Krauss, M.L. Bolognesi, A. Minarini, V. Tumiatti, F. Hucho, C. Melchiorre, Structure-activity relationships of methoctramine-related polyamines as muscular nicotinic receptor noncompetitive antagonists. 2. Role of polymethylene chain lengths separating amine functions and of substituents on the terminal nitrogen atoms., J. Med. Chem. 45 (2002) 1860–1878.

[48] M. Rosini, R. Budriesi, M.G. Bixel, M.L. Bolognesi, A. Chiarini, F. Hucho, P. Krogsgaard-Larsen, I.R. Mellor, A. Minarini, V. Tumiatti, P.N.R. Usherwood, C. Melchiorre, Design, Synthesis, and Biological Evaluation of Symmetrically and Unsymmetrically Substituted Methoctramine-Related Polyamines as Muscular Nicotinic Receptor Noncompetitive Antagonists, J. Med. Chem. 42 (1999) 5212–5223. doi:10.1021/jm991110n.

[49] A. Cavalli, R. Buonfiglio, C. Ianni, M. Masetti, L. Ceccarini, R. Caves, M.W.Y.

Chang, J.S. Mitcheson, M. Roberti, M. Recanatini, Computational design and discovery of “minimally structured” hERG blockers., J. Med. Chem. 55 (2012) 4010–4014. doi:10.1021/jm201194q.

[50] P. Minetti, M.O. Tinti, P. Carminati, M. Castorina, M.A. Di Cesare, S. Di Serio, G. Gallo, O. Ghirardi, F. Giorgi, L. Giorgi, G. Piersanti, F. Bartoccini, G. Tarzia, 2-n-butyl-9-methyl-8-[1,2,3]triazol-2-yl-9H-purin-6-ylamine and analogues as A2A adenosine receptor antagonists. Design, synthesis, and pharmacological characterization, J. Med. Chem. 48 (2005) 6887–6896. doi:10.1021/jm058018d.

[51] M.M. Hann, Molecular obesity, potency and other addictions in drug discovery, Medchemcomm. 2 (2011) 349–355. doi:10.1039/C1MD00017A.

[52] P.W. Kenny, Comment on the Ecstasy and Agony of Assay Interference Compounds, J. Chem. Inf. Model. 57 (2017) 2640–2645. doi:10.1021/acs.jcim.7b00313.

[53] D. Lagorce, O. Sperandio, J. Baell, M. Miteva, B. Villoutreix, FAFDrugs4, (n.d.). http://fafdrugs4.mti.univ-paris-diderot.fr (accessed September 10, 2017).

[54] D.J. Abraham, J. Blagg, Structural Alerts for Toxicity, Burger’s Med. Chem. Drug Discov. (2010). doi:10.1002/0471266949.bmc128.

[55] Glide, Schrödinger Suite 2015-4: version 6.9, Schrödinger, LLC, New York, NY, 2015;, (n.d.).

[56] C. Borsari, R. Lucian, C. Pozz, I. Poehner, S. Henrich, M. Trande, A. Cordeiro-Da-silva, N. Santarem, C. Baptista, A. Tait, F. Di Pisa, L. Dello Iacono, G. Landi, S. Gul, M. Wolf, M. Kuzikov, B. Ellinger, J. Reinshagen, G. Witt, P. Gribbon, M. Kohler, O. Keminer, B. Behrens, L. Costantino, P.T. Nevado, E. Bifeld, J. Eick, J. Clos, J. Torrado, M.J. Corral, J. Alunda, F. Pellati, R.C. Wade, S. Ferrari, S. Mangani, M.P. Costi, Profiling of flavonol derivatives for the development of antitrypanosomatidic drugs, J. Med. Chem. 59 (2016) 7598–7616. doi:10.1021/acs.jmedchem.6b00698.

[57] P. Linciano, C. Pozzi, L. Dello Iacono, F. Di Pisa, G. Landi, A. Bonucci, S. Gul, M. Kuzikov, B. Ellinger, G. Witt, N. Santarem, C. Baptista, C. Franco, C.B. Moraes, W. Müller, U. Wittig, R. Luciani, A. Sesenna, A. Quotadamo, S. Ferrari, I. Pöhner, A. Cordeiro-Da-Silva, S. Mangani, L. Costantino, M.P. Costi, Enhancement of Benzothiazoles as Pteridine Reductase-1 Inhibitors for the Treatment of Trypanosomatidic Infections, J. Med. Chem. 62 (2019) 3989–4012. doi:10.1021/acs.jmedchem.8b02021.

[58] G. Wider, L. Dreier, Measuring Protein Concentrations by NMR Spectroscopy, J. Am.

Chem. Soc. 128 (2006) 2571–2576. doi:10.1021/ja055336t.

[59] P.S.C. Wu, G. Otting, Rapid pulse length determination in high-resolution NMR., J. Magn. Reson. 176 (2005) 115–119. doi:10.1016/j.jmr.2005.05.018.

[60] V. Mesguiche, R.J. Parsons, C.E. Arris, J. Bentley, F.T. Boyle, N.J. Curtin, T.G. Davies, J.A. Endicott, A.E. Gibson, B.T. Golding, R.J. Griffin, P. Jewsbury, L.N. Johnson, D.R. Newell, M.E.M. Noble, L.Z. Wang, I.R. Hardcastle, 4-Alkoxy-2,6-diaminopyrimidine derivatives: Inhibitors of cyclin dependent kinases 1 and 2, Bioorganic Med. Chem. Lett. 13 (2003) 217–222. doi:10.1016/S0960-894X(02)00884-3.

[61] T. Fischer, T. Krüger, A. Najjar, F. Totzke, C. Schächtele, W. Sippl, C. Ritter, A. Hilgeroth, Discovery of novel substituted benzo-anellated 4-benzylamino pyrrolopyrimidines as dual EGFR and VEGFR2 inhibitors, Bioorganic Med. Chem. Lett. 27 (2017) 2708–2712. doi:10.1016/j.bmcl.2017.04.053.

[62] Maestro, Schrödinger Release 2015-4: version 10.4, Schrödinger, LLC, New York, NY, 2015, (n.d.).

[63] Schrödinger Release 2015-4: Schrödinger Suite 2015-4 Protein Preparation Wizard; Epik version 3.4, Schrödinger, LLC, New York, NY, 2015; Impact version 6.9, Schrödinger, LLC, New York, NY, 2015; Prime version 4.2, Schrödinger, LLC, New York, NY, 2015, (n.d.).

[64] E.J. Shanks, H.B. Ong, D.A. Robinson, S. Thompson, N. Sienkiewicz, A.H. Fairlamb, J.A. Frearson, Development and validation of a cytochrome c-coupled assay for pteridine reductase 1 and dihydrofolate reductase, Anal. Biochem. 396 (2010) 194–203. doi:10.1016/j.ab.2009.09.003.

[65] P. Linciano, C.B. Moraes, L.M. Alcantara, C.H. Franco, B. Pascoalino, L.H. Freitas-Junior, S. Macedo, N. Santarem, A. Cordeiro-da-Silva, S. Gul, G. Witt, M. Kuzikov, B. Ellinger, S. Ferrari, R. Luciani, A. Quotadamo, L. Costantino, M.P. Costi, Aryl thiosemicarbazones for the treatment of trypanosomatidic infections, Eur. J. Med. Chem. 146 (2018) 423–434. doi:10.1016/j.ejmech.2018.01.043.

[66] F. Di Pisa, G. Landi, L. Dello Iacono, C. Pozzi, C. Borsari, S. Ferrari, M. Santucci, N. Santarem, A. Cordeiro-da-Silva, C.B. Moraes, L.M. Alcantara, V. Fontana, L.H. Freitas-Junior, S. Gul, M. Kuzikov, B. Behrens, I. Pöhner, R.C. Wade, M.P. Costi, S. Mangani, Chroman-4-One Derivatives Targeting Pteridine Reductase 1 and Showing Anti-Parasitic Activity, Molecules. 22 (2017) 426. doi:10.3390/molecules22030426.

[67] C. Borsari, M.D. Jiménez-antón, J. Eick, E. Bifeld, J. José, A.I. Olías-molero, M.J. Corral, N. Santarem, L. Severi, S. Gul, M. Wolf, M. Kuzikov, B. Ellinger, J. Reinshagen, G. Witt, P. Linciano, A. Tait, L. Costantino, L. Rosaria, P.T. Nevado, D. Zander-dinse, C.H. Franco, S. Ferrari, C.B. Moraes, A. Cordeiro-da-silva, G. Ponterini, Discovery of a benzothiophene-flavonol halting miltefosine and antimonial drug resistance in Leishmania parasites through the application of medicinal chemistry, screening and genomics, Eur. J. Med. Chem. (2019) 111676. doi:10.1016/j.ejmech.2019.111676.

[68] T. Bowling, L. Mercer, R. Don, R. Jacobs, B. Nare, Application of a resazurin-based high-throughput screening assay for the identification and progression of new treatments for human african trypanosomiasis, Int. J. Parasitol. Drugs Drug Resist. 2 (2012) 262–270. doi:10.1016/j.ijpddr.2012.02.002.